



Investigation of Failure Mechanism of Inclined Coal Pillars: Numerical Modelling and Tensorial Statistical Analysis with Field Validations

Arka Jyoti Das^{1,2} · Partha Sarathi Paul² · Prabhat Kumar Mandal¹ · Ranjan Kumar¹ · Subhashish Tewari¹

Received: 11 August 2020 / Accepted: 23 March 2021 / Published online: 17 April 2021
© The Author(s), under exclusive licence to Springer-Verlag GmbH Austria, part of Springer Nature 2021

Abstract

Analysis of the failure mechanism of inclined coal pillars is one of the complicated issues. The wide variability of dip angles of inclined coal pillars makes it more complex. The asymmetric stress distribution and the tendency of shearing along the bedding planes make the inclined coal pillars to behave differently from the flat coal pillars. There is a need for in-depth investigation of the failure mechanism for addressing the instability problems of the inclined coal pillars. Most of the literature quantifies only the magnitudes of the mean principal stresses by classical statistics. As the stress is a second-order tensor having six independent components, the classical statistics is not appropriate to calculate the mean and variability of the principal stresses at the onset of failure of the pillars. In this paper, a comprehensive analysis is done to understand the complex failure mechanism of the inclined coal pillar using numerical modelling as well as tensorial statistics and validated the results with field measurement data of failure cases. The failure mechanism is analysed by quantification of the characteristics of the inclined coal pillars by the principal-stress magnitude and its orientation, induced at the time of failure. Since the spatial variability of the magnitudes and orientations of the induced principal stresses exist within the inclined coal pillars, the mean induced principal stresses ($\bar{\sigma}_1$, $\bar{\sigma}_2$ and $\bar{\sigma}_3$) are used to quantify the stress states within it. The failure stress states within the coal pillars having different dip angles are generated by the calibrated elasto-plastic numerical modelling with the ubiquitous joint model. Several statistical parameters are calculated to quantify the stress-tensor variability and the correlation among the stress-tensor components. It is found that the correlation coefficients among the shear components increase significantly with the increase of the coal pillar dip angle. Therefore, the inclined coal pillars are highly susceptible to shear failure. The magnitudes, as well as orientations of the mean induced principal stresses within the coal pillars obtained through numerical modelling, are quantified by the tensorial as well as classical statistics. It is found that the magnitude of the mean major induced principal stress ($\bar{\sigma}_1$) at the time of failure, i.e. the strength of the pillar decreases with the increase of the dip angles. The validation of the results with the actual stress measurement data shows that all the failed pillar cases are correctly predicted by the tensorial statistical approach whereas the classical statistical approach does not effectively predict the actual failed condition of the pillars. The study would help to characterise the behaviour of the inclined pillars and address the instability issues for safe and efficient mining of inclined coal seams.

Keywords Pillar strength · Inclined coal pillar · Tensorial statistics · Induced principal stresses · Bedding planes · Dip angle · Stress tensor

✉ Prabhat Kumar Mandal
pkmandal@gmail.com

Arka Jyoti Das
arkajyoti19@gmail.com

Partha Sarathi Paul
drpspaul@iitism.ac.in

Ranjan Kumar
ranjan4k@gmail.com

Subhashish Tewari
tewari_s@yahoo.com

¹ CSIR-Central Institute of Mining and Fuel Research,
Dhanbad 826001, India

² Indian Institute of Technology (Indian School of Mines),
Dhanbad 826004, India

List of Symbols

IPS	Induced principal stresses within the pillar
\mathbf{T}	Stress tensor matrix
$\bar{\mathbf{T}}$	Mean stress tensor matrix
σ, τ	Normal and shear components of stress tensor
$\sigma_1, \sigma_2, \sigma_3$	Major, intermediate and minor principal stresses
$\bar{\sigma}_1, \bar{\sigma}_2, \bar{\sigma}_3$	Mean major, intermediate and minor principal stresses
Ω_S	Variance matrix of individual tensor component
N	Numbers of hexahedral elements within the numerical model of the coal pillar
φ	Azimuth counted from the north (i.e. Y -axis) in the clockwise direction
θ	Plunge counted with respect to the horizontal plane and is positive for upward direction
$\bar{\varphi}$	Mean azimuth
$\bar{\theta}$	Mean plunge
\tilde{l}_x, m, n	Direction cosine along X, Y and Z axis
\tilde{t}^i	Stress vector of the i th element
$\tilde{\mu}_i$	Mean stress vector
Σ_i	Covariance matrix
Ω_{Ed}	Euclidean dispersion
$tr()$	Trace of a matrix
$\det()$	Determinant of a matrix
$\ \cdot \ $	Frobenius norm or Euclidean norm
\tilde{x}	Direction vector
$\tilde{\mu}$	Mean direction vector
σ_H, σ_h	Major and minor horizontal in situ stresses
σ_v	Vertical in situ stresses
H	Depth of cover
S	Flat coal pillar strength
σ_c	Intact strength of the coal
h	Coal pillar height
w	Coal pillar width
\mathbf{T}^i	Half-vectorisation of stress tensor matrix $\text{vech}(\mathbf{T}^i)$
Ω_g	Generalised variance
Ω_{Eff}	Effective variance
Ω_{total}	Total variance
MCSS	Mohr–Coulomb strain softening

1 Introduction

The analysis of the stress field during the excavation is essential to assess the stability of the underground structures. As the rockmass is in a stressed condition due to the existence of the in situ stresses, the excavation causes the redistribution of the in situ stress field. It changes not only the magnitude but also the orientation of the stress tensor. Along with the magnitude, the orientation of the stress

tensor is a major factor for the underground structures stability assessment (Arthur et al. 1980; Zou and Kaiser 1990; Martin 1997; Martin and Kaiser 1999; Kaiser et al. 2001; Diederichs et al. 2004; Shen et al. 2018; Bai et al. 2019; Yao et al. 2019; Xu and Arson 2015; Li et al. 2019; Yan et al. 2020). As the stability is evaluated by the principal stresses induced due to the excavation, it is required to estimate their magnitudes and the orientation in and around the excavation.

The induced principal stresses (IPS) show spatial variability in the magnitude and the orientation. The variability of stress is significant in coal pillars. When the coal pillars are on the verge of failure, the stress is more at the core and gradually decreases toward the edges from the core (Das et al. 2019a, b). Due to the spatial variability in the stresses, the difficulties are faced during the calculation of the magnitude and orientation of the mean IPS ($\bar{\sigma}_1, \bar{\sigma}_2$ and $\bar{\sigma}_3$) at the onset of failure of the coal pillar. The mean IPS ($\bar{\sigma}_1, \bar{\sigma}_2$ and $\bar{\sigma}_3$) not only represents the statistical characteristics of the stress data but also describe the overall stress conditions in a coal pillar (Cantieni and Anagnostou 2009; Koptev 2013; Siren et al. 2015; Han et al. 2016). Though numerical modelling is found to be a suitable tool to evaluate the stress tensor in the coal pillar, it gives the magnitude and orientation of the IPS at each zone/element. Since stress is a second-order tensor having six independent components, the classical statistics, used for the scalar or vector quantities, cannot be applied to calculate the mean, variance and other statistical parameters (Gao and Harrison 2018a, 2019; Feng et al. 2019). The classical statistics separately calculate the magnitude and orientation of the IPS. Therefore, the interrelation between the magnitude and the orientation of the IPS are not addressed by classical statistics. The variability of the stress within the coal pillar is quantified by the dispersion, which is usually measured by the standard deviation for scalar or vector data in classical statistics (Gao and Harrison 2018b; Lei and Gao 2019). Hence, the tensorial statistics are required to analyse the failure mechanism for dealing with the stress–tensor components for quantification of the variability and the mean of the IPS within the coal pillars.

The behaviour of inclined coal pillars is dissimilar and more complex than the flat coal pillars due to the variability of dip angles, asymmetric stress distribution and the tendency of shearing along the bedding planes. For addressing the instability problems of inclined coal pillars, there is a need to investigate the failure mechanism of inclined coal pillars. The tensorial statistics found to be the right tool for the analysis of the failure mechanism of inclined coal pillars. Gao and Harrison (2017, 2018a, b, 2019) studied the variability in the measurement of the in situ stresses by tensorial statistics. They found that the classical statistics are not appropriate for the analysis of the stress tensor because it considers the principal stresses magnitudes and their orientations as independent quantities and ignores the

inter-relation between them. The mean calculated by the classical statistics does not maintain the orthogonality of the principal stresses. They showed the procedures to calculate the mean principal stresses by the tensorial statistics. A multivariate distribution model of the second-order stress tensor was proposed in their study to quantify the variability of stress tensors. As the study is performed on the in situ stress data, it does not illustrate the magnitudes, orientations and variability of the IPS due to the excavation. However, this approach can be extended to understand the complex nature of stress condition induced in the inclined coal pillars at the onset of failure.

Das et al. (2019b) showed that the distribution of stress in the flat coal pillar is almost symmetric but it is highly asymmetric for the inclined coal pillar. They found that the magnitude of the mean major IPS ($\overline{\sigma_1}$) in the flat coal pillars is very close to the mean vertical stress component of the stress tensor. When the dip angle of the coal pillar increases, the magnitude of the mean vertical stress component decreases and the shear components along the bedding planes increase. The shearing characteristics arise due to the tendency of the rockmass to slide along the inclined bedding planes. But, their study does not quantify the orientation of the mean major IPS ($\overline{\sigma_1}$) within the coal pillar at the time of failure.

Most of the literature (Wang et al. 2017, 2020; Mohan et al. 2001; Seo et al. 2016; Wu et al. 2020; Jaiswal and Shrivastva 2009; Shabanimashcool and Li 2013; Mandal et al. 2020) mainly emphasised the magnitude of the IPS on the coal pillars, induced due to the extraction of the coal seam. In their study, the mean of the IPS was calculated by classical statistics. The orientation or directional aspects of the IPS were not mentioned in these studies. Limited literature is found which studied the orientation of the IPS within the coal pillars or the surrounding rockmass due to the excavation (Foroughi 1996; Eberhardt 2001; Maritz 2015; Ptáček 2015). Eberhardt (2001) studied the rotation of the principal stresses ahead of the tunnel face during the excavation. He carried out three-dimensional finite element modelling to analyse the near-field stress during the sequential excavation of the tunnel. He found that the damage in the surrounding rockmass depends on the amount of stress rotation. He considered the rotation of the principal stresses during sequential advancement at some particular points ahead of the tunnel face. His study does not describe the procedure to calculate the magnitude and orientation of the mean IPS.

It is found from the literature that the inclined coal pillar behaves differently than the flat coal pillar as the inclined rock strata show spatial variability in the stress and complex directional failure characteristics (Das et al. 2019a, b). Thus, the study of the failure mechanism and the stress state within the inclined coal pillars are needed for a better understanding of its characteristics. The literature does not

suitably describe the quantification of the magnitude and the orientation of the mean IPS ($\overline{\sigma_1}$, $\overline{\sigma_2}$ and $\overline{\sigma_3}$) within the inclined pillars on the verge of failure. In this paper, the characteristics of the inclined pillars are studied by quantifying the magnitude and the orientation of the mean IPS ($\overline{\sigma_1}$, $\overline{\sigma_2}$ and $\overline{\sigma_3}$) at the time of failure in which the mean major IPS ($\overline{\sigma_1}$) represents the strength of the coal pillar. The elasto-plastic numerical simulation with the ubiquitous joint constitutive model is carried out by FLAC3D (Itasca 2017) to generate the stress tensor within the inclined pillar at the time of failure. The ubiquitous joint constitutive model is capable to simulate the failure behaviour of the rock strata along the inclined bedding planes. The values of the stress components within the inclined coal pillar are obtained at each zone/element of the numerical model. The mean IPS ($\overline{\sigma_1}$, $\overline{\sigma_2}$ and $\overline{\sigma_3}$) within the inclined coal pillars are calculated from the array of the stress tensor data by the tensorial as well as classical statistics. The spatial variability of the stress tensor, the correlation and the covariance among the stress–tensor elements are calculated for the coal pillars of different dip angles. A comparison is carried out between the results obtained by the tensorial as well as classical statistics. The change of the magnitude and the orientation of the mean IPS ($\overline{\sigma_1}$, $\overline{\sigma_2}$ and $\overline{\sigma_3}$) are shown for the different inclinations of the coal pillar. The validation of the failure mechanism of the inclined pillars is carried out by the failed coal pillar cases where the induced stress is measured in different underground coal mines.

2 Mean and Variability of the IPS by Classical Statistics

In three dimensions, the stresses in an object are represented by the second-order tensor of a 3×3 matrix as given below:

$$\mathbf{T} = \begin{bmatrix} \sigma_{xx} & \tau_{xy} & \tau_{xz} \\ \tau_{yx} & \sigma_{yy} & \tau_{yz} \\ \tau_{zx} & \tau_{zy} & \sigma_{zz} \end{bmatrix}, \quad (1)$$

where τ and σ are the shear and normal components, respectively. In this stress tensor, the components $\tau_{xy} = \tau_{yx}$, $\tau_{xz} = \tau_{zx}$ and $\tau_{yz} = \tau_{zy}$. Thus, the tensor \mathbf{T} becomes symmetric. The eigenvectors and eigenvalues of tensor \mathbf{T} give the orientation and the magnitude of the principal stresses, respectively, in an object (Brady and Brown 1993). At the onset of failure of the inclined coal pillar, the stress tensor (\mathbf{T}) is not similar at each location of the inclined coal pillar. It results in different magnitude and the orientation of the IPS within the inclined pillar. The stress tensor within the inclined pillar can be denoted as follows:

$$T^i = \begin{bmatrix} \sigma_{xx}^i & \tau_{xy}^i & \tau_{xz}^i \\ \text{Symmetry} & \sigma_{yy}^i & \tau_{yz}^i \\ & & \sigma_{zz}^i \end{bmatrix} \tag{2}$$

Here, i denotes the hexahedral zones as shown in Fig. 1. The eigenvalues and the eigenvectors give the magnitude and the orientation of the IPS, respectively, at each block. The mean of the IPS can be calculated by classical statistics as follows:

$$\bar{\sigma}_1 = \frac{1}{N} \sum_{i=1}^{i=N} \sigma_1^i; \bar{\sigma}_2 = \frac{1}{N} \sum_{i=1}^{i=N} \sigma_2^i; \bar{\sigma}_3 = \frac{1}{N} \sum_{i=1}^{i=N} \sigma_3^i, \tag{3}$$

where $\bar{\sigma}_1, \bar{\sigma}_2$ and $\bar{\sigma}_3$ are the mean major, mean intermediate and mean minor IPS respectively within the inclined coal pillar; σ_1^i, σ_2^i and σ_3^i are the major, intermediate and minor IPS respectively in the i th block of the inclined coal pillar.

In classical statistics, the variances of the stress–tensor component are calculated independently by processing each component. In the Cartesian coordinate system, the mean values of the shear components are zero by definition. Equation (4) shows the dispersion of individual tensor component with respect to its mean.

$$\Omega_s = \frac{1}{N-1} \begin{bmatrix} \sum_{i=1}^{i=N} (\sigma_{xx}^i - \bar{\sigma}_{xx})^2 & \sum_{i=1}^{i=N} (\tau_{xy}^i)^2 & \sum_{i=1}^{i=N} (\tau_{xz}^i)^2 \\ \text{Symmetry} & \sum_{i=1}^{i=N} (\sigma_{yy}^i - \bar{\sigma}_{yy})^2 & \sum_{i=1}^{i=N} (\tau_{yz}^i)^2 \\ & & \sum_{i=1}^{i=N} (\sigma_{zz}^i - \bar{\sigma}_{zz})^2 \end{bmatrix} \tag{4}$$

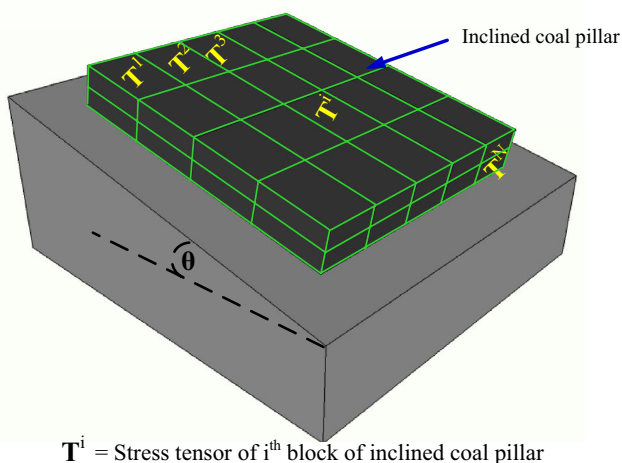


Fig. 1 Schematic diagram of the inclined coal pillar having different stress tensor within it

where N is the number of the block within the inclined coal pillar.

The overall dispersion of the stress tensor about its mean is not quantified by the Eq. (4). The variance in the magnitude of the IPS is expressed by the following equation:

$$\begin{aligned} \text{var}(\sigma_1) &= \frac{1}{N} \sum (\sigma_1^i - \bar{\sigma}_1)^2; \text{var}(\sigma_2) \\ &= \frac{1}{N} \sum (\sigma_2^i - \bar{\sigma}_2)^2; \text{var}(\sigma_3) \\ &= \frac{1}{N} \sum (\sigma_3^i - \bar{\sigma}_3)^2. \end{aligned} \tag{5}$$

The orientation of the IPS is quantified by the azimuth and plunge. The azimuth and the plunge can be represented by a point on the surface of a sphere. The azimuth $\varphi \in [0, 2\pi]$ is counted from the north (i.e. Y-axis) in a clockwise direction. The plunge $\theta \in [-\frac{\pi}{2}, \frac{\pi}{2}]$ is counted with respect to the horizontal plane and is positive for upward direction. In Cartesian coordinate, the orientation is represented by the direction cosines. The direction cosines are obtained from the azimuth and the plunge by the following equation:

$$l = \cos \theta \sin \varphi; m = \cos \theta \cos \varphi; n = \sin \theta, \tag{6}$$

where l, m and n signify the direction cosine along X-, Y- and Z-axis, respectively. These also denote the unit vector of a line along X-, Y- and Z-axis, respectively. The orientations of the IPS at each block of the inclined coal pillar (Fig. 1) are obtained by the eigenvector of the stress tensor T^i . The mean orientation of the IPS is calculated as follows (Davis 1986; Fisher et al. 1993):

$$\bar{l} = \frac{\sum_{i=1}^{i=N} l^i}{R}; \bar{m} = \frac{\sum_{i=1}^{i=N} m^i}{R}; \bar{n} = \frac{\sum_{i=1}^{i=N} n^i}{R}, \tag{7}$$

where l^i, m^i and n^i are the direction cosine of the IPS in the i th block of the inclined coal pillar; \bar{l}, \bar{m} and \bar{n} are the mean direction cosine of the IPS in the inclined coal pillar and $R = \sqrt{(\sum_{i=1}^{i=N} l^i)^2 + (\sum_{i=1}^{i=N} m^i)^2 + (\sum_{i=1}^{i=N} n^i)^2}$ measures the concentration of the spherical data.

After calculating the mean direction cosines of the IPS, the mean azimuth ($\bar{\varphi}$) and the mean plunge ($\bar{\theta}$) are obtained as follows:

$$\left\{ \begin{aligned} \bar{\varphi} &= \begin{cases} \text{mod} \left[\left\{ 2\pi + \tan^{-1} \left(\bar{l}/\bar{m} \right) \right\}, 2\pi \right] & \text{if } \bar{m} \geq 0 \\ \pi + \tan^{-1} \left(\bar{l}/\bar{m} \right) & \text{if } \bar{m} < 0 \end{cases} \\ \bar{\theta} &= \sin^{-1}(\bar{n}) \end{aligned} \right. \quad (8)$$

The spherical variance of the orientation data of the IPS is expressed by the following equation:

$$\text{var}(\varphi, \theta) = \left(1 - \frac{R}{N} \right), \quad (9)$$

where N is the number of data points.

3 Mean and Variability of the IPS by Tensorial Statistics

As per the tensorial statistics, the stress should be analysed in the common Cartesian coordinate in the Euclidean space. In Euclidean space, the arithmetic mean between two points lies at the mid-point of the line joining the two points. Euclidean mean stress is calculated by averaging each tensor component. Euclidean mean stress tensor ($\bar{\mathbf{T}}$) within the inclined coal pillar can be written as follows (Walker et al. 1990):

$$\bar{\mathbf{T}} = \frac{1}{N} \sum_{i=1}^{i=N} \mathbf{T}^i = \frac{1}{N} \begin{bmatrix} \sum_{i=1}^{i=N} \sigma_{xx}^i & \sum_{i=1}^{i=N} \tau_{xy}^i & \sum_{i=1}^{i=N} \tau_{xz}^i \\ \sum_{i=1}^{i=N} \tau_{xy}^i & \sum_{i=1}^{i=N} \sigma_{yy}^i & \sum_{i=1}^{i=N} \tau_{yz}^i \\ \sum_{i=1}^{i=N} \tau_{xz}^i & \sum_{i=1}^{i=N} \tau_{yz}^i & \sum_{i=1}^{i=N} \sigma_{zz}^i \end{bmatrix}$$

$$= \begin{bmatrix} \bar{\sigma}_{xx} & \bar{\tau}_{xy} & \bar{\tau}_{xz} \\ \text{Symmetry} & \bar{\sigma}_{yy} & \bar{\tau}_{yz} \\ \text{Symmetry} & \text{Symmetry} & \bar{\sigma}_{zz} \end{bmatrix} \quad (10)$$

The eigenvectors and the eigenvalues of the matrix $\bar{\mathbf{T}}$ give the orientations and the magnitudes of the mean IPS ($\bar{\sigma}_1, \bar{\sigma}_2$ and $\bar{\sigma}_3$), respectively.

As the matrix \mathbf{T}^i is symmetric, the half-vectorisation gives a column vector which consists of six components of the stress tensor (Seber 2007). The half-vectorisation can be written by the following expression:

$$\tilde{\mathbf{t}}^i = \text{vech}(\mathbf{T}^i) = [\sigma_{xx}^i \ \tau_{xy}^i \ \tau_{xz}^i \ \sigma_{yy}^i \ \tau_{yz}^i \ \sigma_{zz}^i]^T \quad (11)$$

The mean stress vector $\tilde{\boldsymbol{\mu}}_t$ can be obtained from Eq. (10) as follows:

$$\tilde{\boldsymbol{\mu}}_t = \text{vech}(\bar{\mathbf{T}}) = [\bar{\sigma}_{xx} \ \bar{\tau}_{xy} \ \bar{\tau}_{xz} \ \bar{\sigma}_{yy} \ \bar{\tau}_{yz} \ \bar{\sigma}_{zz}]^T \quad (12)$$

The covariance matrix of the six stress components are as follows (Johnson 2002):

$$\Sigma_t = \frac{1}{N-1} \sum_{i=1}^{i=N} (\tilde{\mathbf{t}}^i - \tilde{\boldsymbol{\mu}}_t)(\tilde{\mathbf{t}}^i - \tilde{\boldsymbol{\mu}}_t)^T,$$

$$= \frac{1}{N-1} \begin{bmatrix} \text{var}(\sigma_{xx}) & \text{cov}(\sigma_{xx}, \tau_{xy}) & \text{cov}(\sigma_{xx}, \tau_{xz}) & \text{cov}(\sigma_{xx}, \sigma_{yy}) & \text{cov}(\sigma_{xx}, \tau_{yz}) & \text{cov}(\sigma_{xx}, \sigma_{zz}) \\ \text{Symmetry} & \text{var}(\tau_{xy}) & \text{cov}(\tau_{xy}, \tau_{xz}) & \text{cov}(\tau_{xy}, \sigma_{yy}) & \text{cov}(\tau_{xy}, \tau_{yz}) & \text{cov}(\tau_{xy}, \sigma_{zz}) \\ \text{Symmetry} & \text{Symmetry} & \text{var}(\tau_{xz}) & \text{cov}(\tau_{xz}, \sigma_{yy}) & \text{cov}(\tau_{xz}, \tau_{yz}) & \text{cov}(\tau_{xz}, \sigma_{zz}) \\ \text{Symmetry} & \text{Symmetry} & \text{Symmetry} & \text{var}(\sigma_{yy}) & \text{cov}(\sigma_{yy}, \tau_{yz}) & \text{cov}(\sigma_{yy}, \sigma_{zz}) \\ \text{Symmetry} & \text{Symmetry} & \text{Symmetry} & \text{Symmetry} & \text{var}(\tau_{yz}) & \text{cov}(\tau_{yz}, \sigma_{zz}) \\ \text{Symmetry} & \text{Symmetry} & \text{Symmetry} & \text{Symmetry} & \text{Symmetry} & \text{var}(\sigma_{zz}) \end{bmatrix}, \quad (13)$$

$$= \frac{1}{N-1} \begin{bmatrix} \sum_{i=1}^{i=N} (\sigma_{xx}^i - \bar{\sigma}_{xx})^2 & \sum_{i=1}^{i=N} (\sigma_{xx}^i - \bar{\sigma}_{xx})(\tau_{xy}^i - \bar{\tau}_{xy}) & \sum_{i=1}^{i=N} (\sigma_{xx}^i - \bar{\sigma}_{xx})(\tau_{xz}^i - \bar{\tau}_{xz}) & \sum_{i=1}^{i=N} (\sigma_{xx}^i - \bar{\sigma}_{xx})(\sigma_{yy}^i - \bar{\sigma}_{yy}) & \sum_{i=1}^{i=N} (\sigma_{xx}^i - \bar{\sigma}_{xx})(\tau_{yz}^i - \bar{\tau}_{yz}) & \sum_{i=1}^{i=N} (\sigma_{xx}^i - \bar{\sigma}_{xx})(\sigma_{zz}^i - \bar{\sigma}_{zz}) \\ \sum_{i=1}^{i=N} (\tau_{xy}^i - \bar{\tau}_{xy})^2 & \sum_{i=1}^{i=N} (\tau_{xy}^i - \bar{\tau}_{xy})(\tau_{xz}^i - \bar{\tau}_{xz}) & \sum_{i=1}^{i=N} (\tau_{xy}^i - \bar{\tau}_{xy})(\sigma_{yy}^i - \bar{\sigma}_{yy}) & \sum_{i=1}^{i=N} (\tau_{xy}^i - \bar{\tau}_{xy})(\tau_{yz}^i - \bar{\tau}_{yz}) & \sum_{i=1}^{i=N} (\tau_{xy}^i - \bar{\tau}_{xy})(\sigma_{zz}^i - \bar{\sigma}_{zz}) \\ \sum_{i=1}^{i=N} (\tau_{xz}^i - \bar{\tau}_{xz})^2 & \sum_{i=1}^{i=N} (\tau_{xz}^i - \bar{\tau}_{xz})(\sigma_{yy}^i - \bar{\sigma}_{yy}) & \sum_{i=1}^{i=N} (\tau_{xz}^i - \bar{\tau}_{xz})(\tau_{yz}^i - \bar{\tau}_{yz}) & \sum_{i=1}^{i=N} (\tau_{xz}^i - \bar{\tau}_{xz})(\sigma_{zz}^i - \bar{\sigma}_{zz}) \\ \sum_{i=1}^{i=N} (\sigma_{yy}^i - \bar{\sigma}_{yy})^2 & \sum_{i=1}^{i=N} (\sigma_{yy}^i - \bar{\sigma}_{yy})(\tau_{yz}^i - \bar{\tau}_{yz}) & \sum_{i=1}^{i=N} (\sigma_{yy}^i - \bar{\sigma}_{yy})(\sigma_{zz}^i - \bar{\sigma}_{zz}) \\ \sum_{i=1}^{i=N} (\tau_{yz}^i - \bar{\tau}_{yz})^2 & \sum_{i=1}^{i=N} (\tau_{yz}^i - \bar{\tau}_{yz})(\sigma_{zz}^i - \bar{\sigma}_{zz}) \\ \sum_{i=1}^{i=N} (\sigma_{zz}^i - \bar{\sigma}_{zz})^2 \end{bmatrix}$$

The variability of the stress tensor is measured by the Euclidean dispersion and the multivariate dispersion. In multivariate statistics, the dispersion of the stress–tensor matrix is quantified by three ways i.e., total variation, generalized variance and effective variance.

The Euclidean dispersion (Ω_{Ed}) of a matrix is written as follows:

$$\Omega_{Ed} = \frac{1}{N} \sum_{i=1}^N \|T^i - \bar{T}\|^2, \quad (14)$$

where $\|\cdot\|$ is the Frobenius norm or Euclidean norm (Horn 2013).

The total variation (Ω_{total}), generalized variance (Ω_g) and effective variance (Ω_{eff}) of a stress tensor are given by the following equations (Peña and Rodríguez 2003):

$$\Omega_{total} = tr(\Sigma_t), \quad (15)$$

$$\Omega_g = \det(\Sigma_t), \quad (16)$$

$$\Omega_{eff} = \frac{1}{2} p^{(p+1)} \sqrt{\Omega_g}, \quad (17)$$

where $tr()$ is the trace of a matrix, $\det()$ is the determinant of a matrix, p is the dimension of a matrix. For 3-D cases, the dimension of the stress–tensor matrix is 3.

4 Design of Numerical Modelling

The complete stress tensor (all components of stress tensor) at the onset of failure of the coal pillars having different dip angles is generated by simulating the compressive testing of the inclined coal pillars. The numerical simulation is performed to obtain the stress–strain curve under similar conditions to the uniaxial compressive strength (UCS) in a universal testing machine (UTM) at the laboratory. The coal pillars are uniaxially compressed between the upper and the lower rock formation of the coal pillar which serve the purpose of platens analogous to the platens of a UTM. A full coal pillar is simulated for each dip angle to understand the stress conditions at the onset of failure of a pillar. The upward and downward movements of the platens are allowed during the UCS testing at the laboratory. In the numerical modelling, the boundary conditions represent a similar condition of the UCS testing in a UTM. Most of the published papers used roller boundary conditions at the lateral boundaries for the simulation of an inclined pillar (Lorig and Cabrera 2013; Ma et al. 2016; Jessu et al. 2018; Jessu and Spearing 2019; Garza-Cruz et al. 2019). Lorig and Cabrera (2013) suggested to simulate the symmetry of

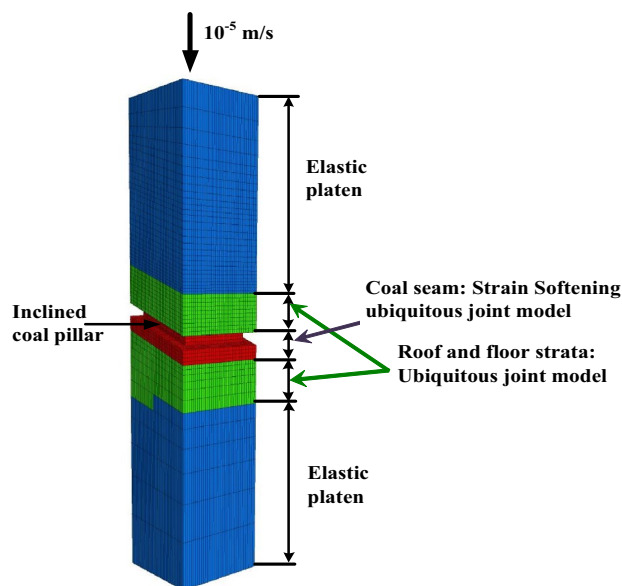


Fig. 2 Constitutive models used in numerical modelling

the inclined coal pillars either by keeping the boundaries far enough to avoid its influence on the results or using the periodic boundary condition. The periodic boundary conditions assume infinite arrays of pillars. Thus, the periodic boundary conditions are applied at the lateral boundaries and the bottom of the model is fixed along the z direction. Mizzi et al. (2020) discussed the implementation of the periodic boundary conditions in numerical modelling. At the top of the model, a constant compressive velocity of 10^{-5} m/s is applied to move the upper and the lower strata along the vertical direction as shown in Fig. 2 (Das et al. 2017, 2019b; Mandal et al. 2008).

4.1 Constitutive Models of Rockmass used in Numerical Simulation

The presence of bedding planes plays a major role in the anisotropic characteristics of the coal measure rocks. The inclined rock strata have the shear failure propensity along the bedding planes. This characteristic of the inclined rock strata is suitably simulated by the ubiquitous joint model. The failure modes simulated by this constitutive model are (a) rock matrix failure by shear and tension and (b) the sliding failure along the bedding planes (Das et al. 2017, 2019b). The failure characteristics of the rock matrix and bedding planes are simulated independently in the numerical modelling (Das et al. 2019b) by incorporating the directional failure criterion for anisotropic characteristics of bedding planes within the elasto-plastic rockmass failure criterion.

The coal pillar is modelled by the Mohr–Coulomb constitutive model with strain softening (MCSS) for matrix

failure which is coupled with the ubiquitous joint model for sliding along the bedding planes. The upper and the lower rock formation up to fifteen metres (i.e. five times the coal pillar's height) are modelled by assigning the elasto-plastic MC model along with the ubiquitous joints model. The elastics model is considered for the rest of the strata which resembles the stiff platens of a UTM. Figure 2 illustrates the constitutive models of the rockmass used in the numerical simulation of the UCS testing on the pillars with the width-to-height ratio of 3.5. The height and width of the pillar as shown in Fig. 2 are considered as 3.0 m and 10.5 m, respectively. The cohesion, friction angle, direction of dip and dip angle of the existing bedding planes are the input parameters of the ubiquitous joint model. In this constitutive model, the failure along the bedding planes and the rock matrix failure are checked separately during each iteration step and accordingly, the stress states are updated in the numerical models. The stress state within the inclined coal pillar is analysed at the onset of failure to quantify their characteristics.

4.2 Determination of Rockmass Properties from the Intact Rock Properties

The proper estimation of the required input parameters determines the accuracy of the numerical simulation. For the simulation of underground excavation, the intact rock properties found from the laboratory testing cannot be used directly as it does not represent the rockmass at actual field conditions. The proper conversion of laboratory tested intact rock properties to rockmass properties is needed for effective numerical modelling of field conditions (Das et al. 2017, 2019b; Mandal et al. 2008).

The various input parameters required for the numerical simulation by MCSS with ubiquitous joint constitutive mode are (a) elastic constants, i.e. Poisson's ratio and Young's modulus, (b) cohesions and friction angles (peak and residual values), (c) post-peak characteristics of the rock matrix, i.e. strain-softening parameters, (d) in situ stresses and (e) properties of the bedding planes, i.e. dip angle, dip direction, friction angle and cohesion. Das et al. (2017, 2019a, b) suggested to consider the values of bedding planes friction angle and its cohesion as 24° and 0.18 MPa, respectively for the

Table 1 Intact rock properties

Rock type	Thickness (m)	Young's modulus (GPa)	Density (kg/m ³)	UCS (MPa)	BTS (MPa)
Cgsst	4.23	3.7	2210	24	1.6
IA seam	1.07	1.8	1580	22.1	2.3
Shale	0.69	2.3	1580	19.5	1.3
Cgsst	3.52	3.7	2200	24	1.7
Carbonaceous shale	0.6	1.7	1500	21.1	1.41
Cgsst	3	2.85	2195	18.88	1.72
Fgsst	0.72	5.2	2440	49.6	6.9
Cgsst	5.28	3.5	2140	15.31	1.64
Fgsst	2.89	4.1	2270	24.8	2.5
Cgsst	0.85	2.4	2190	15.6	1.83
I seam	1.3	1.9	1580	24.5	2.4
Cgsst	17.6	3.53	2246	23.13	2.54
II seam	5.08	1.8	1580	22.5	2.4
Mgsst	13.51	2.72	2203	22.97	2.67
Fgsst	0.32	3.9	2310	34.1	3.7
LB1 seam	0.45	2	1580	20.1	2.4
Mgsst	9.29	3.6	2210	23.83	2.02
IIIB seam	1.25	2.0	1580	18.9	2.4
Carbonaceous shale	13.07	4.0	2138	14.45	1.33
IIIA seam	1.2	2.0	1580	25	2.4
Cgsst (immediate roof)	8.26	5.3	2286	21.36	2.02
<i>Salarjung coal seam (coal pillar)</i>	<i>7.45</i>	<i>2.0</i>	<i>1580</i>	<i>18.9</i>	<i>1.26</i>
Cgsst (floor)	50	3.3	2190	18.5	1.23

Cgsst coarse-grained sandstone, *Fgsst* fine-grained sandstone, *Mgsst* medium-grained sandstone, *UCS* uniaxial compressive strength, *BTS* Brazilian tensile strength, Poisson's ratio of the rock strata is considered as 0.25. The coal pillar is simulated for the Salarjung coal seam as highlighted in bold and italics

coal measures strata in Indian geominig conditions. These values are used to simulated the shearing characteristics of bedding planes by the ubiquitous joint model. The intact properties of the laboratory scale rock samples are shown in Table 1 which are converted to the rockmass properties by the Sheorey’s rockmass failure criterion (Sheorey 1997). The internal friction angle and the cohesion for the rockmass are calculated by this failure criterion. Bieniawski RMR (Bieniawski 1976) is used in this criterion to estimate the rockmass properties by converting the laboratory strength properties of intact rock.

Sheorey’s rockmass failure criterion (Sheorey 1997) is written as follows:

$$\sigma_{1m} = \sigma_{cm} \left(1 + \frac{\sigma_{3m}}{\sigma_{tm}}\right)^{b_m}, \tag{18}$$

$$\left. \begin{aligned} \sigma_{cm} &= \sigma_{ci} e^{\left(\frac{RMR-100}{20}\right)} \\ \sigma_{tm} &= \sigma_{ti} e^{\left(\frac{RMR-100}{27}\right)} \\ b_m &= b \frac{RMR}{100} \end{aligned} \right\}, \tag{19}$$

where σ_j is the tri-axial strength (MPa); σ_3 is the confining stress (MPa); σ_c is the compressive strength (MPa); σ_t is the tensile strength (MPa); b is equal to 0.51 which is constant in the failure criterion obtained from triaxial test data, and RMR is the Bieniawski Rock Mass Rating (Bieniawski 1976). The subscript m and i in the above equations represent the rockmass and the intact rock, respectively.

The failure envelop of the rockmass is expressed by the Eq. (20) where τ is the shear strength of the rockmass (MPa), σ is the normal stress (MPa), μ_{0m} is the coefficient of friction of the rockmass, ϕ_{0m} is the internal friction angle of the rockmass.

$$\tau = \tau_{sm} \left(1 + \frac{\sigma}{\sigma_{tm}}\right)^{c_m}, \tag{20}$$

where

$$\tau_{sm} = \left(\sigma_{cm} \sigma_{tm} \frac{b_m^{b_m}}{(1 + b_m)^{1+b_m}}\right)^{1/2}, \tag{21}$$

$$\mu_{0m} = \frac{\tau_{sm}^2 (1 + b_m)^2 - \sigma_{tm}^2}{2\tau_{sm} \sigma_{tm} (1 + b_m)}, \tag{22}$$

$$\begin{aligned} c_m &= \mu_{0m}^{0.9} \frac{\sigma_{tm}}{\tau_{sm}}, \\ \mu_{0m} &= \tan \phi_{0m}. \end{aligned} \tag{23}$$

Various researchers (Kushwaha et al. 2010; Mandal et al. 2008; Das et al. 2017, 2019b) used this non-linear failure criterion for successful simulation of underground coal mining-related problems.

4.3 Consideration of In Situ Stresses

The failure of a coal pillar significantly depends on the in situ stresses conditions. The mean in seam horizontal in situ stress is predicted by Sheorey (1994). The value of the major (σ_H) and minor (σ_h) components of the horizontal in situ stresses (MPa) are obtained as follows:

$$\sigma_H = \sigma_h = \frac{\nu}{1 - \nu} \sigma_v + \frac{\beta EG}{1 - \nu} (H + 1000), \tag{24}$$

where ν is the Poisson’s ratio, H is the depth of cover (m), β is the coefficient of thermal expansion ($^{\circ}C$), E is the Young’s modulus (GPa), G is the geothermal gradient ($^{\circ}C/m$).

The vertical in situ stress is calculated as follows:

$$\sigma_v = 0.025H. \tag{25}$$

Equation (24) has good agreement with the in situ stress measurement data (Sheorey et al. 2001). The mean value of the in situ horizontal stress of Indian coal measures rock is calculated by putting the values of $G = 3 \times 10^{-2} \text{ }^{\circ}C/m$, $\nu = 0.25$, $E = 2 \text{ GPa}$, $\beta = 0.00003/^{\circ}C$ as per Sheorey et al. (2001). Thus, Eq. (24) can be written as follows:

$$\sigma_H = \sigma_h = 2.4 + 0.01H. \tag{26}$$

Equations (25) and (26) are used to calculate in situ stresses which are the input parameters for the numerical simulation. These equations have successfully been used in different studies (Mohan et al. 2001; Kushwaha and Banerjee 2005; Singh et al. 2011; Mandal et al. 2008; Kushwaha et al. 2010; Das et al. 2017, 2019b) to simulate the practical coal mining problems.

Table 2 Rate of cohesion and internal friction angle drop with respect to plastic shear strain

Plastic shear strain	Cohesion (MPa)	Internal friction angle (deg)
0.0	0.23	42.15
0.06	0.01	37
0.08	0.0	35
0.1	0.0	35

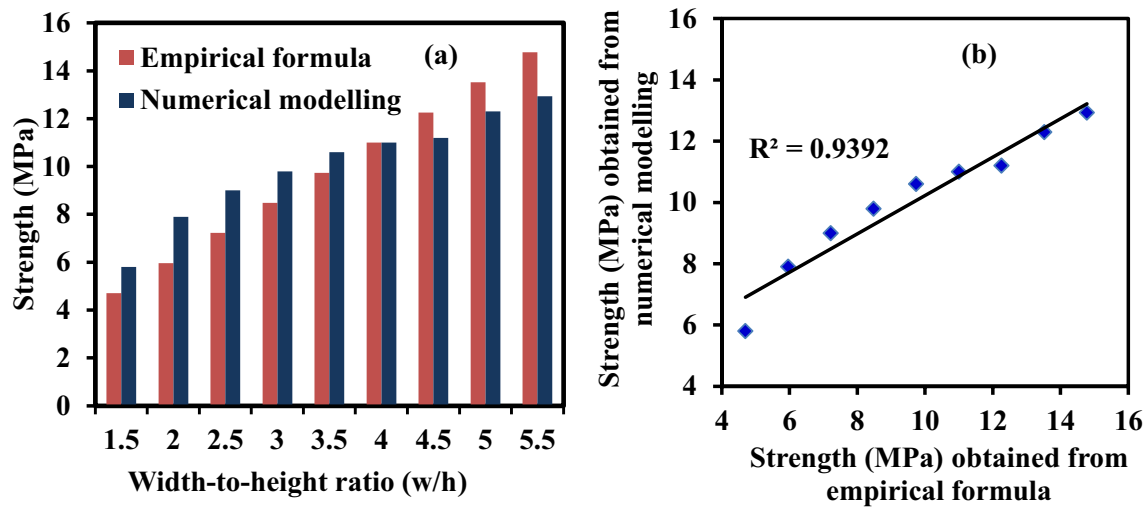


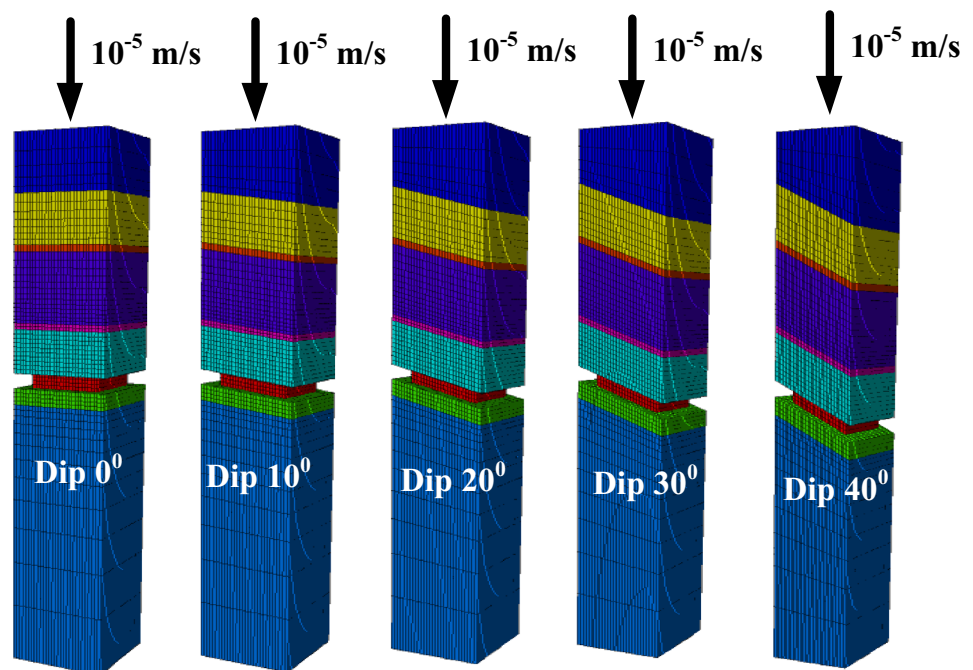
Fig. 3 Comparison between the strength obtained by the numerical modelling and by the empirical formula for calibration of MCSS parameters

4.4 Calibration of MCSS Parameters for the Numerical Simulation

UCS testing of pillars with the different width-to-height ratio is simulated to calibrate and generate suitable MCSS parameters, i.e. cohesion and internal friction angle drop with respect to the plastic strain. The zone size of the coal pillar is kept as $0.5 \text{ m} \times 0.5 \text{ m} \times 0.5 \text{ m}$ in the numerical models. The calibration of the MCSS parameters for the coal seam is carried out with this zone size. The zone sizes along the x and y directions of the lower and upper strata are also

kept as $0.5 \text{ m} \times 0.5 \text{ m} \times 0.5 \text{ m}$. But, the zone size along the z-direction of the lower and upper strata is varied with the ratio 0.8 and 1.1, respectively, to make denser zones near to the coal seam. Several trial numerical models are run to find proper MCSS parameters so that the values of pillar strength obtained by the numerical simulation are near to the values obtained by the empirical strength formula for different width-to-height ratio. The pillar strength formula as given in Eq. (27) (Sheorey et al. 1987; Sheorey 1992) is used to calibrate the MCSS parameters.

Fig. 4 Grid used in numerical modelling for parametric study



$$S = 0.27\sigma_{ci}h^{-0.36} + \left(\frac{H}{250} + 1\right)\left(\frac{w}{h} - 1\right), \quad (27)$$

where S is the strength of the flat coal pillar (MPa), σ_{ci} is the laboratory strength of the coal sample (MPa), h is the coal pillar height (m), w is the coal pillar width (m), H is the depth cover (m).

Table 2 shows the calibrated MCSS parameters. Figure 3 shows the comparison between the strength obtained by the empirical formulation and by the numerical simulation studies. The R^2 value, i.e. the coefficient of determination between the numerically and empirically obtained pillar strength is 0.94 as shown in Fig. 3b. The well-calibrated input parameters are used for the simulation of actual field conditions and the parametric study.

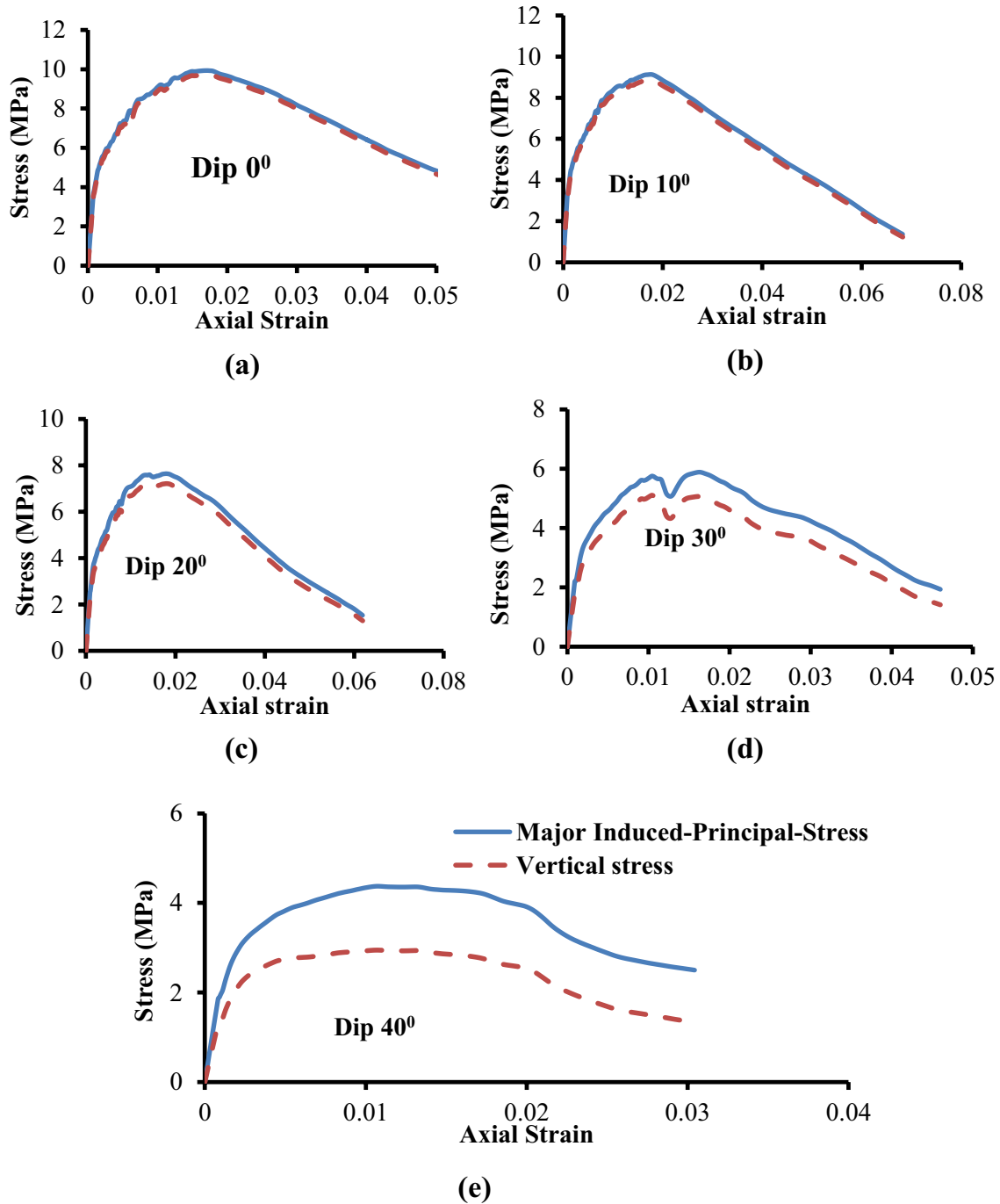


Fig. 5 Major IPS (σ_1) and vertical stress vs. axial strain curve of the coal pillar for a Dip 0°, b Dip 10°, c Dip 20°, d Dip 30° and e Dip 40°

5 Parametric Study

After calibration of the MCSS parameters, the parametric study is carried out by varying dip angles of the coal pillars from 0° to 40° at an interval of 10° for the pillars of width-to-height ratio 3.5. Figure 4 shows the grid of the numerical modelling of the incline coal pillars having the height and width as 3.0 m and 10.5 m, respectively. The numerical models are simulated as per the rock formations of the Shanthikhani Mine, one of the inclined mine of Singareni Collieries Company Limited (SCCL), India as shown in Table 1. The numerical UCS test is performed by the calibrated MCSS parameters to obtain the failure stress state within the inclined coal pillars. This parametric study helps to quantify the effects of the dip of the pillars on the stress state within the pillar.

6 Results of Numerical Modelling

Figure 5 illustrates the stress–strain curve obtained during the loading process of the pillar in numerical modelling. In this figure, the major IPS (σ_1) and the vertical stress within the inclined coal pillar are averaged by the classical statistics at each iteration step and plotted with the corresponding axial strain. It is obtained from this figure that the difference between the mean major IPS ($\overline{\sigma_1}$) and the mean vertical stress is less in the case of a flat coal pillar. But, as the inclination of the pillar increases, the difference in magnitude between the mean major IPS ($\overline{\sigma_1}$) and the mean vertical

stress with a pillar increases. From this phenomenon, it can be anticipated that the direction of the mean major IPS ($\overline{\sigma_1}$) gradually deviates from the vertical axis as the inclination of the pillar increases.

The analysis is done at the onset of the failure of the pillar, i.e. when the stresses reach the peak. At this stage, the stress state is not uniform within the coal pillar. Figure 6a shows that at the middle of the pillar, the magnitude of the major IPS (σ_1) is high and it gradually decreases towards the edges of the pillar. It is depicted from Fig. 6b, c that two hexahedral zones at different locations in the inclined coal pillar have different orientations of the IPS though their magnitudes are approximately equal. It suggests that the IPS show spatial variability within the inclined coal pillar in respect of magnitude as well as orientation. From the results of the numerical modelling, the stress tensor at each hexahedral zone of the inclined coal pillars is extracted to calculate the magnitude and the orientation of the IPS at each hexahedral zone.

The orientation of the IPS at each hexahedral zone of the coal pillar is represented by the point on the surface of a unit sphere. MATLAB codes are written to plot the directional data on the surface of the three-dimensional unit sphere. Figures 7, 8a and 9a show the direction of the IPS in the coal pillars having different dip angles at the onset of the failure. The dip of the inclined pillar is along the south direction and the rise side of the pillar is along the north direction. It is obtained from Fig. 7 that the points which denote the orientation of the major IPS (σ_1) are concentrated at the pole of the unit sphere in the case of the pillar with dip angle 0° . It indicates that the direction of the major IPS (σ_1) at the

Fig. 6 Contours of the major IPS [σ_1] (Pa) in the coal pillar of the inclination 40° and the variation of the orientation of the principal stresses within it

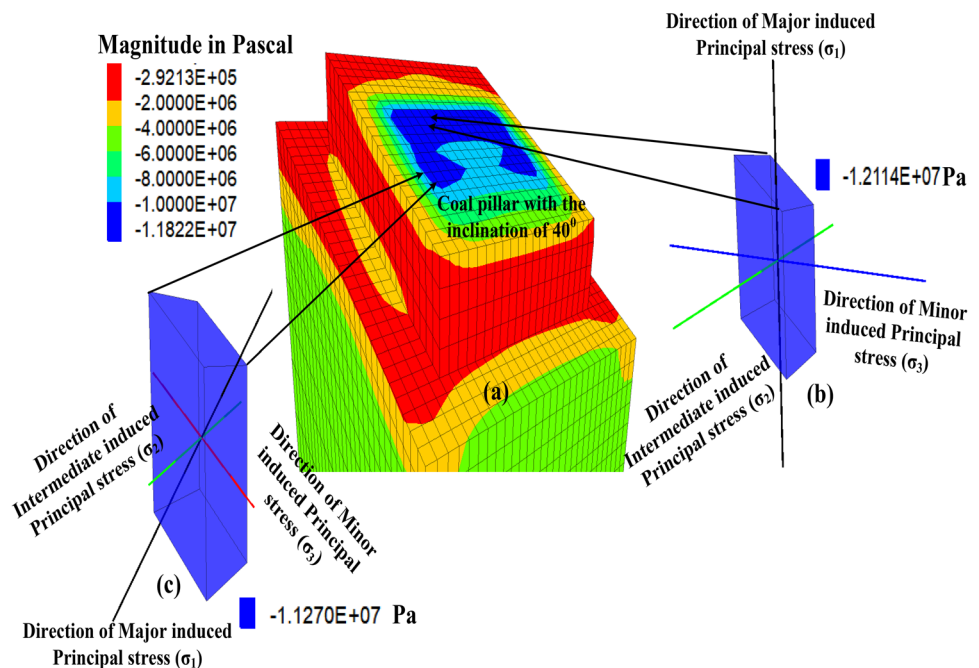
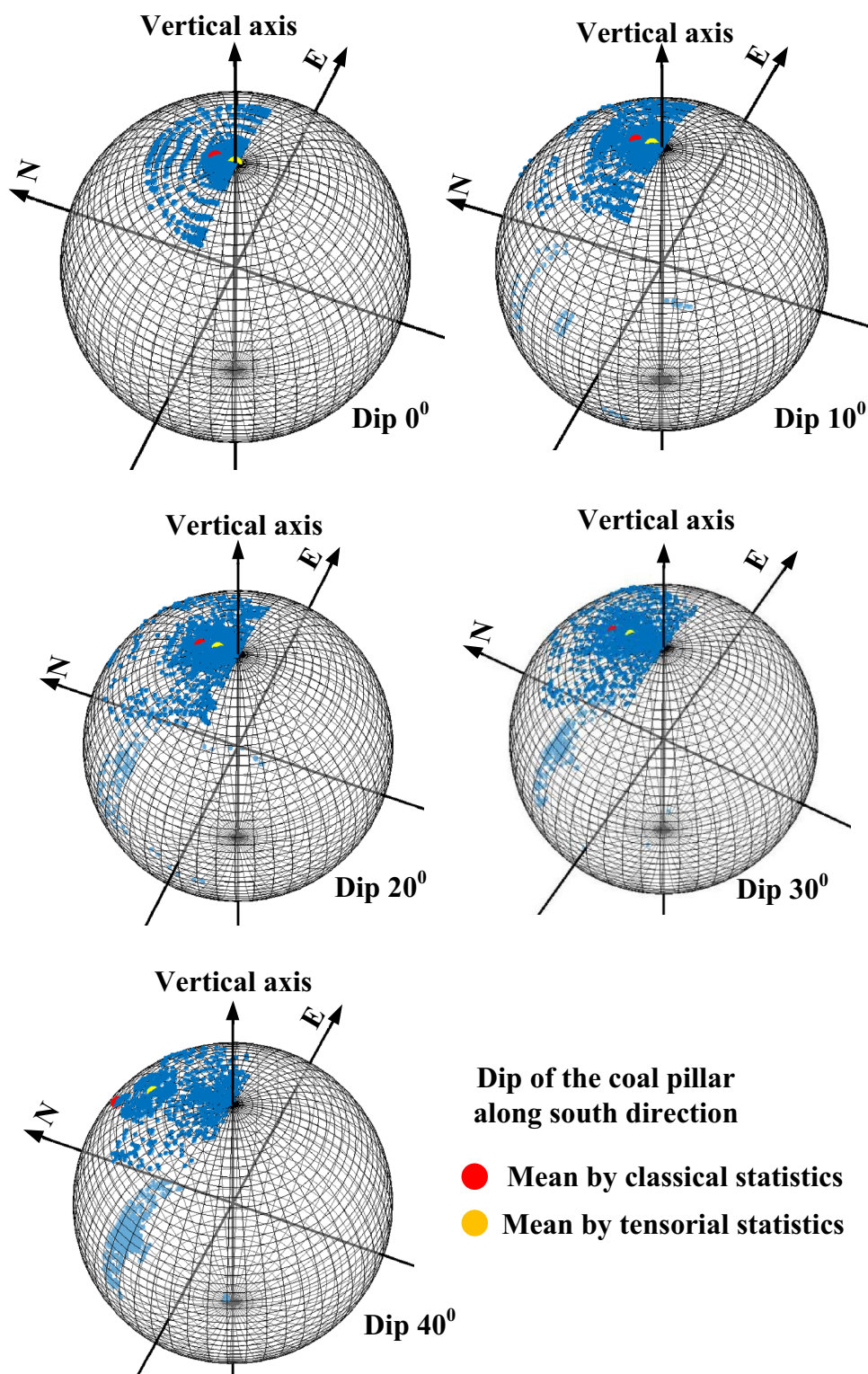


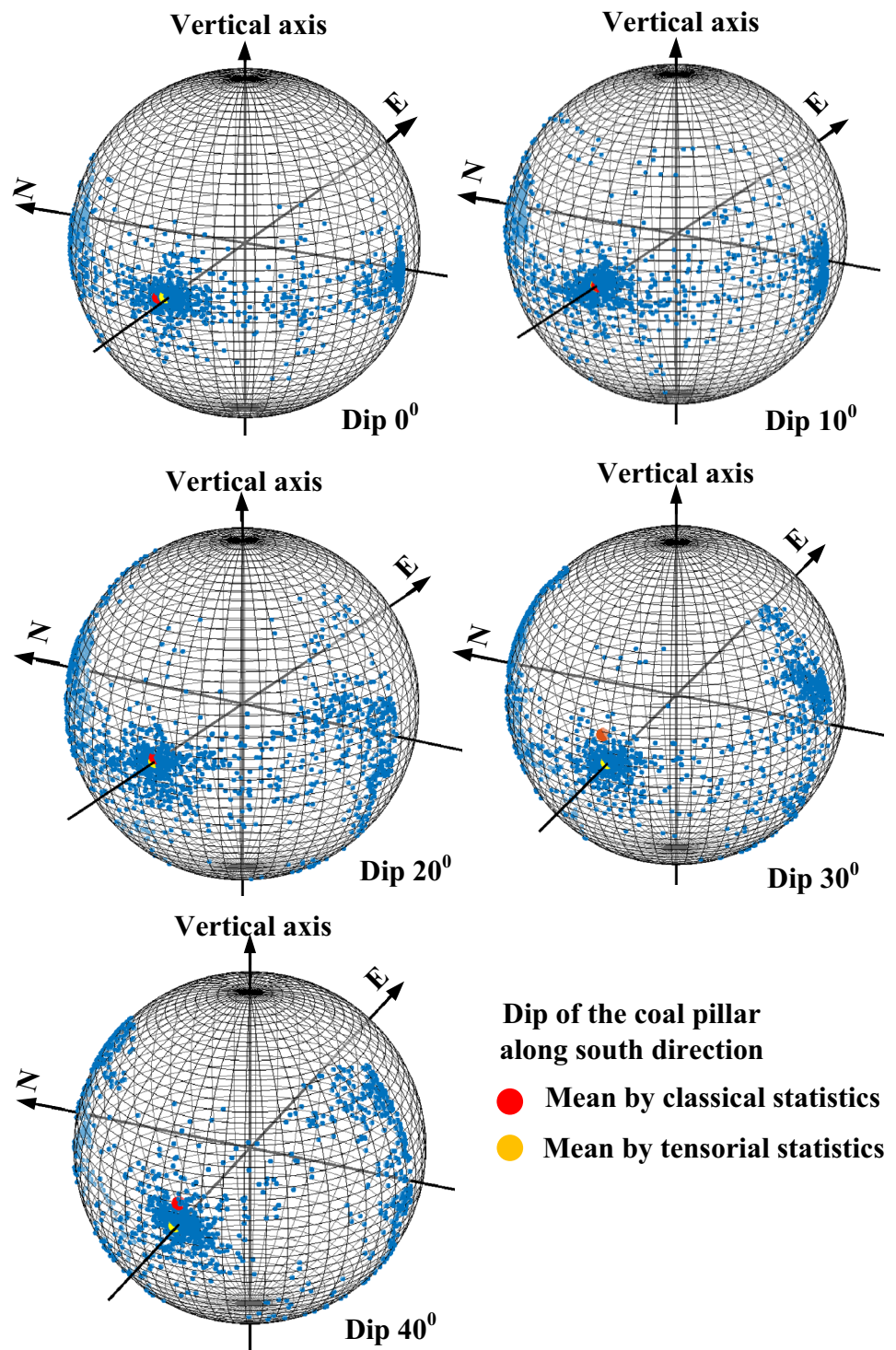
Fig. 7 Direction of the major IPS (σ_1) in the coal pillar with respect to the dip of the coal pillar



onset of failure of the flat pillar is along the vertical axis, i.e. perpendicular to the flat pillar. But as the inclination of the coal pillar increases, the points are shifted from the pole towards the equatorial plane in the north direction which is the direction of the rise side of the inclined pillar. In Figs. 8a

and 9a, the intermediate (σ_2) and minor (σ_3) IPS are scattered in the equatorial plane in the case of a flat pillar. It indicates that the intermediate (σ_2) and minor (σ_3) IPS act in the flat pillar along the horizontal direction. Therefore, the IPS in the flat coal pillar maintains the orthogonality. To comply

Fig. 8 Direction of the intermediate IPS (σ_2) in the coal pillar with respect to the dip of the coal pillar

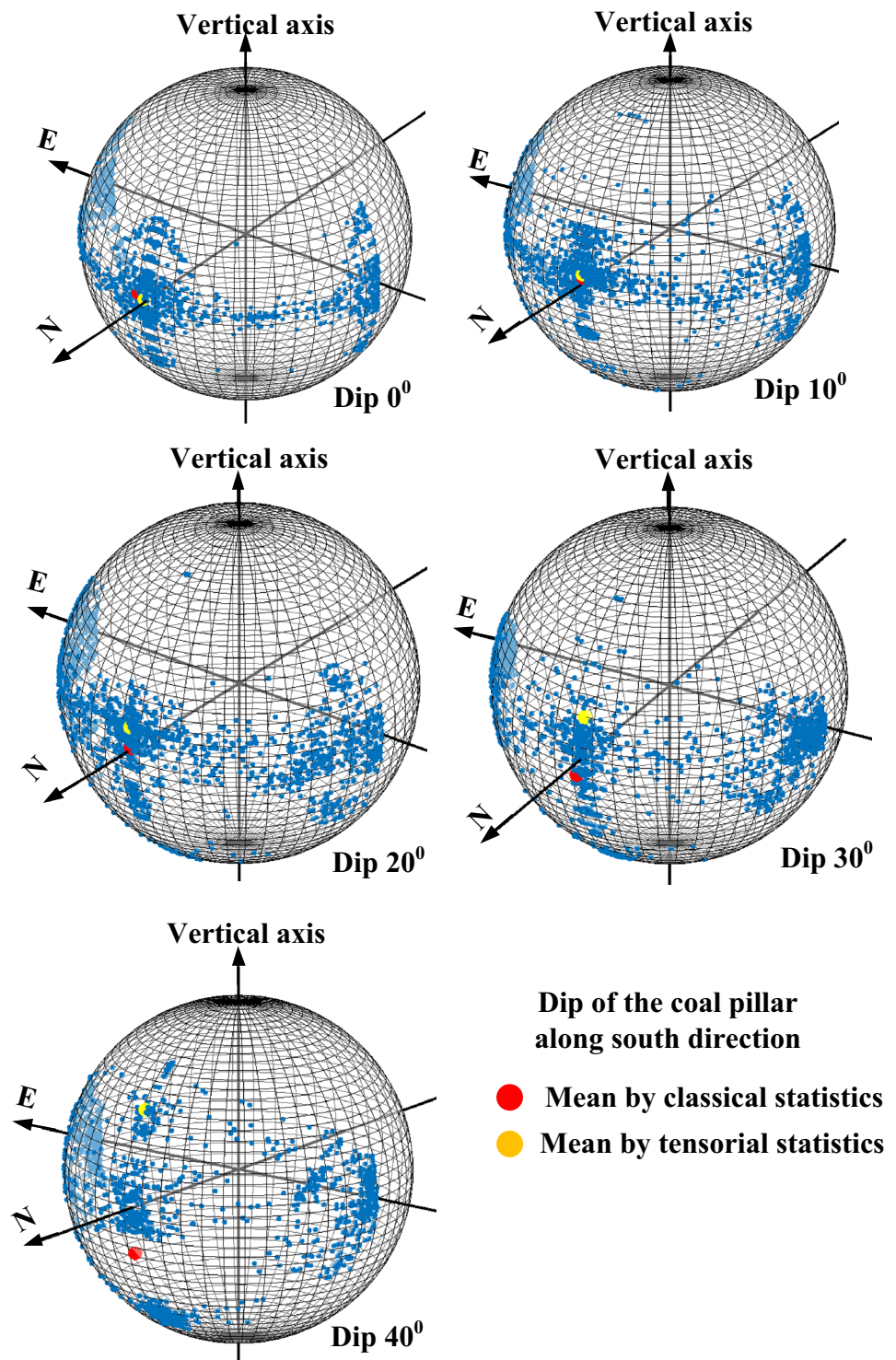


with the orthogonality, the intermediate (σ_2) and minor (σ_3) IPS within the inclined coal pillar deviate from the equatorial plane as shown in Figs. 8 and 9, respectively. The quantification of the mean IPS ($\overline{\sigma_1}$, $\overline{\sigma_2}$ and $\overline{\sigma_3}$) will provide a clear picture of the stress conditions within the inclined pillar.

7 Determination of the Magnitudes of the Mean IPS

The magnitudes of the mean IPS within the coal pillar of different dip angles are quantified by classical and tensorial statistics as given below:

Fig. 9 Direction of the minor IPS (σ_3) in the coal pillar with respect to the dip of the coal pillar



7.1 Calculation of by Classical Statistics

Equation (3) is used to calculate the mean IPS ($\bar{\sigma}_1$, $\bar{\sigma}_2$ and $\bar{\sigma}_3$) by the classical statistics. Figures 10, 11 and 12 show the histogram of the IPS obtained by the classical statistics. It is obtained from these figures that the magnitudes of the mean major IPS ($\bar{\sigma}_1$) at the time of failure, i.e., the strength

of the pillar decrease with the increase of the coal pillar dip angle. Tables 3, 4 and 5 show the descriptive statistics of the IPS within the inclined pillars at the time of failure obtained by the classical statistics. It is found from these tables that the standard deviations of magnitudes of all the three IPS are minimum for inclined coal pillars of dip 40°. The magnitudes of the IPS within the inclined coal pillars at

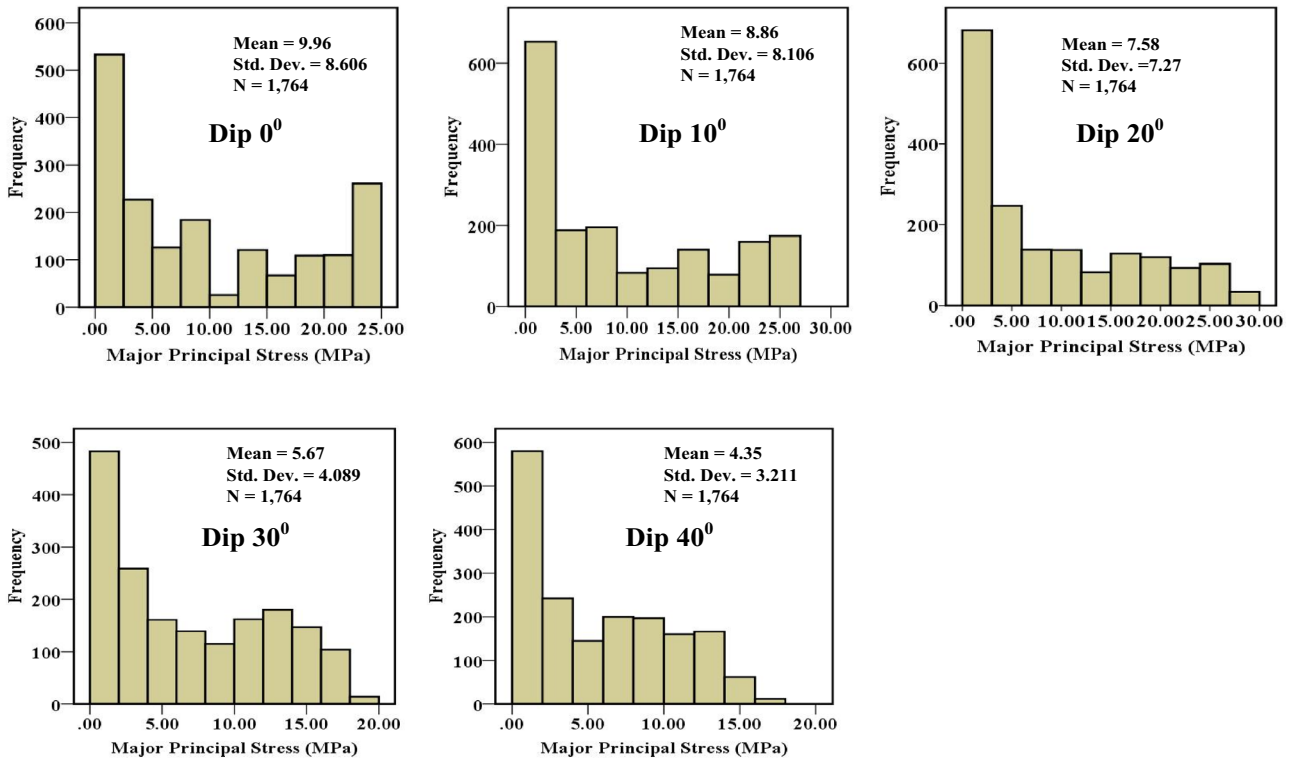


Fig. 10 Histogram of major IPS [σ_1] (MPa) within the inclined coal pillars of different dip angle at the time of failure

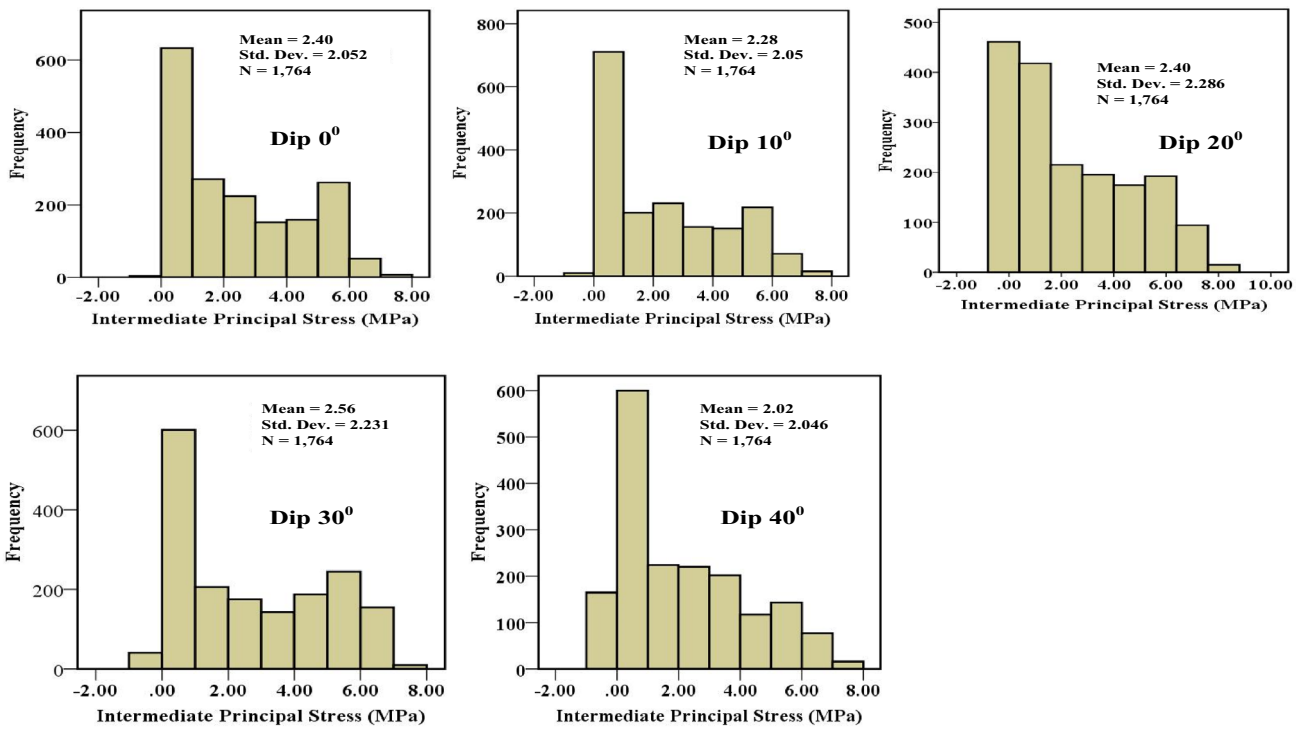


Fig. 11 Histogram of intermediate IPS [σ_2] (MPa) within the inclined coal pillars of different dip angle at the time of failure

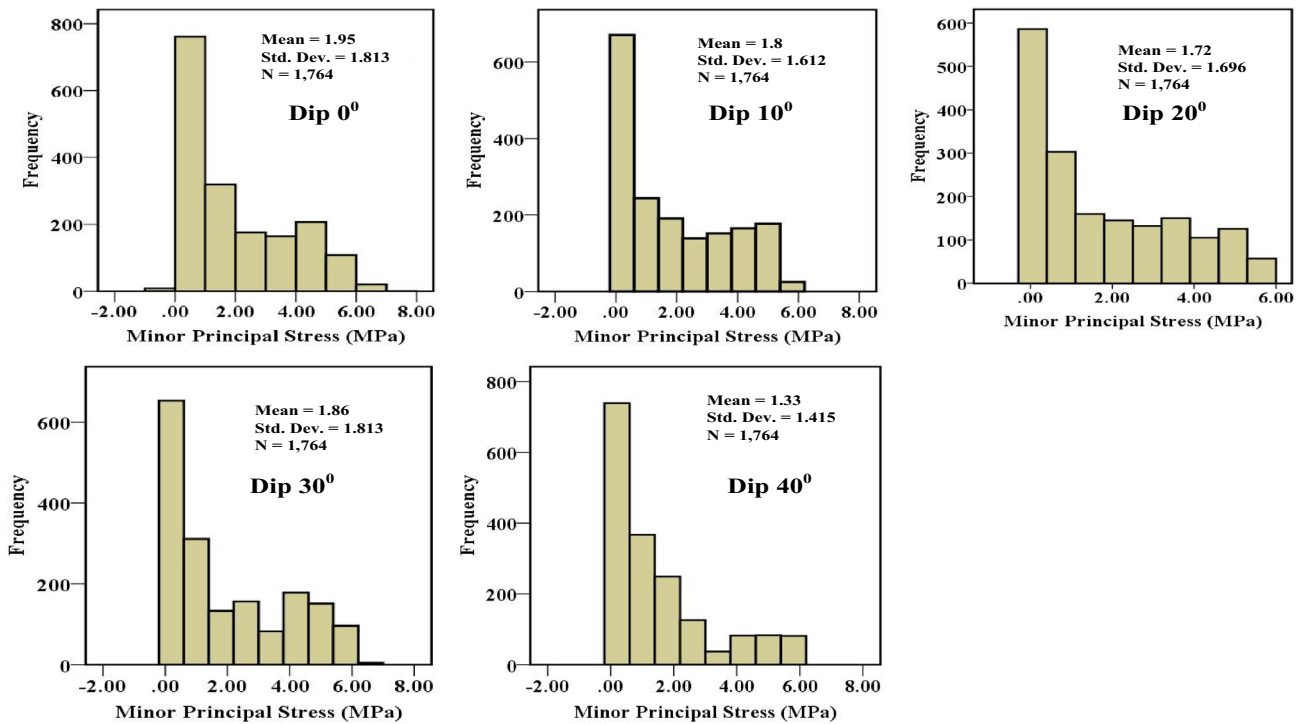


Fig. 12 Histogram of minor IPS [σ_3] (MPa) within the inclined coal pillars of different dip angle at the time of failure

Table 3 Statistical analysis of the major IPS (σ_1) in the inclined coal pillars of different dip angle by classical statistics

	Major induced principal stress (σ_1)				
	Dip 0°	Dip 10°	Dip 20°	Dip 30°	Dip 40°
Mean (MPa)	9.96	8.86	7.58	5.67	4.35
Median (MPa)	7.44	6.56	5.35	5.76	4.99
Mode (MPa)	6.23	6.74	2.08	0.03	11.17
Std. deviation (MPa)	8.60	8.11	7.27	4.09	3.21
Variance (MPa ²)	74.06	77.80	72.57	29.79	21.44
Skewness	0.75	0.60	0.46	0.40	0.45
Kurtosis	-1.34	-1.15	-0.79	-1.23	-1.09

Table 4 Statistical analysis of the intermediate IPS (σ_2) in the inclined coal pillars of different dip angle by classical statistics

	Intermediate induced principal stress (σ_2)				
	Dip 0°	Dip 10°	Dip 20°	Dip 30°	Dip 40°
Mean (MPa)	2.40	2.28	2.40	2.56	2.02
Median (MPa)	1.88	1.76	1.64	2.07	1.52
Mode (MPa)	1.29	1.29	1.12	-0.11	2.35
Std. deviation (MPa)	2.05	2.05	2.29	2.23	2.05
Variance (MPa ²)	4.21	4.36	5.17	5.08	4.11
Skewness	0.50	0.60	0.66	0.36	0.74
Kurtosis	-1.13	-0.95	-0.90	-1.36	-0.61

Table 5 Statistical analysis of the minor IPS (σ_3) in the inclined coal pillars of different dip angle by classical statistics

	Minor induced principal stress (σ_3)				
	Dip 0°	Dip 10°	Dip 20°	Dip 30°	Dip 40°
Mean (MPa)	1.95	1.8	1.72	1.86	1.33
Median (MPa)	1.4	1.26	1.07	1.09	0.93
Mode (MPa)	1.16	1.25	0.36	-0.11	2.21
Std. deviation (MPa)	1.81	1.61	1.70	1.81	1.441
Variance (MPa ²)	3.28	3.07	3.05	3.67	2.79
Skewness	0.64	0.64	0.71	0.70	1.30
Kurtosis	-0.90	-0.98	-0.86	-0.92	0.67

the onset of failure show the positively skewed distribution as shown in Figures 10, 11 and 12. As the skewness value of the major IPS (σ_1) is more for the pillar of dip angle 0°, the distribution of the major IPS (σ_1) is comparatively more skewed in the case of the flat pillar. Similarly, the skewness values of intermediate (σ_2) and minor (σ_3) IPS are more for the pillar of dip angle 40°.

7.2 Calculation by Tensorial Statistics

After obtaining the stress tensor at each hexahedral zone within the inclined coal pillar, the tensorial statistics is applied to estimate the mean values of the IPS. The mean

Table 6 Magnitude of the mean IPS (at the time of failure) in the inclined coal pillars of different dip angles obtained by classical statistics and by tensorial statistics

	$\bar{\sigma}_1$ (MPa)		$\bar{\sigma}_2$ (MPa)		$\bar{\sigma}_3$ (MPa)	
	Classical statistics	Tensorial statistics	Classical statistics	Tensorial statistics	Classical statistics	Tensorial statistics
Dip 0°	9.96	9.74	2.40	2.30	1.95	2.27
Dip 10°	8.86	8.61	2.28	2.25	1.40	1.65
Dip 20°	7.58	7.28	2.40	2.33	1.72	2.06
Dip 30°	5.67	5.24	2.56	2.64	1.86	2.22
Dip 40°	4.35	2.03	2.02	2.12	1.33	1.87

stress tensor (\bar{T}) in the inclined coal pillars is obtained by Eq. (10) whose eigenvalues give the magnitudes of the mean IPS ($\bar{\sigma}_1$, $\bar{\sigma}_2$ and $\bar{\sigma}_3$) within the inclined coal pillars. Table 6 shows the comparison between the magnitudes of the mean IPS ($\bar{\sigma}_1$, $\bar{\sigma}_2$ and $\bar{\sigma}_3$) within the inclined coal pillars at the time of failure obtained by the classical statistics and tensorial statistics. It shows that the values of mean major IPS ($\bar{\sigma}_1$) and intermediate IPS ($\bar{\sigma}_2$) calculated by the tensorial statistics are less than the values calculated by the classical statistics. But, the values of mean minor IPS ($\bar{\sigma}_3$) calculated by the tensorial statistics are more than the values calculated by the classical statistics.

7.3 Determination of the Variability of the Stress Tensor

The variance values of the IPS as given in Tables 3, 4 and 5, describe the variation in the magnitudes of the IPS. These are calculated individually by classical statistics. It does not represent the total variation of the stress tensor within the inclined coal pillars because the classical statistics do not consider the interrelation between other stress components. Therefore, the tensorial statistics are applied to quantify the overall dispersion or variability of the stress tensor within the inclined coal pillars with dip angle 0°–40°. At first, the covariance matrix for the stress tensor of the coal pillars with different dip angles is computed by Eq. (13). The covariance matrices are shown in Appendix. In the covariance matrix, the values along the diagonal line represent the variance of the corresponding stress component. The values of other cells in the covariance matrix represent the covariance between two stress components. In each covariance matrix, the variance of the vertical stress component (σ_{zz}) is more

compared to the variance of other stress components. As the dip of the pillar increases, the variance of the vertical stress component (σ_{zz}) decreases. The variance of the vertical stress component (σ_{zz}) is 77.99 MPa² and 17.18 MPa² for the coal pillar with dip angles 0° and 40°, respectively.

After obtaining the covariance matrix, the overall variation of the stress tensor within the inclined coal pillars are computed by the Eqs. (14)–(17). The values of different variances are tabulated in Table 7. The Euclidean dispersion (Ω_{Ed}) and the total variation (Ω_{total}) of the stress tensor consider only the variances of stress–tensor components. As these ignore the covariance between the tensor components, their values do not represent the total dispersion of the stress tensor. The generalised, as well as effective variances, are more efficient to measure the dispersion of complete stress tensor as these consider the covariance between the tensor components. The higher values of these variances signify more dispersion of the stress tensor with respect to its mean stress tensor. It is found that the variance value is less for the coal pillar with a dip angle of 40° compared to a coal pillar with a dip angle of 0°. It indicates that the stress tensor within the coal pillar having the dip angle 40° is more concentrated to its mean stress tensor in comparison to the coal pillar having the dip angle 0°.

The values in the correlation matrix signify the correlation between two stress components. The correlation matrices are shown in Figures 13, 14, 15, 16 and 17. It is obtained from these figures that the correlation coefficients among σ_{xx} , σ_{yy} and σ_{zz} are more compared to the correlation between other stress components. As the dip of the pillar increases, the correlation among normal stress components (σ_{xx} , σ_{yy} and σ_{zz}) decreases, e.g., the correlation coefficients between σ_{yy} and σ_{zz} is 0.98 and 0.86 for the coal pillar with dip angles 0° and 40°, respectively. It is observed that the

Table 7 Variability of the stress tensor within the inclined coal pillars

	Dip 0°	Dip 10°	Dip 20°	Dip 30°	Dip 40°
Euclidean dispersion (Ω_{Ed}) in (MPa) ²	88.79	84.97	84.92	41.53	31.60
Total variation (Ω_{total}) in (MPa) ²	87.14	83.56	82.74	40.26	29.09
Generalised variance (Ω_g) in (MPa) ¹²	0.27	0.043	0.022	0.01	0.009
Effective variance (Ω_{eff}) in (MPa) ²	0.80	0.59	0.53	0.48	0.35

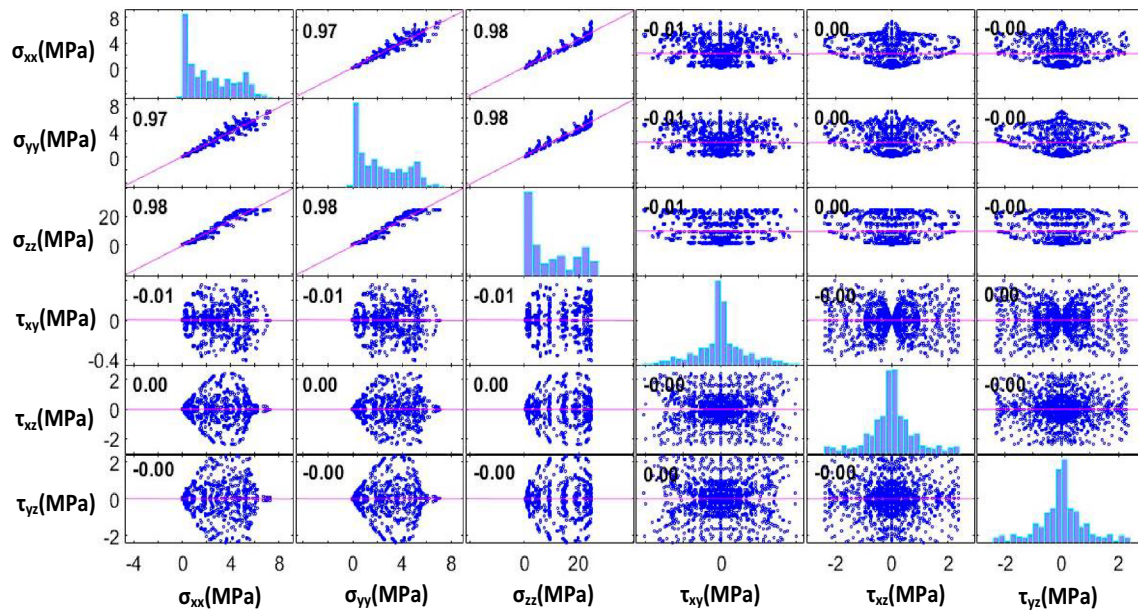


Fig. 13 Correlation matrix for the stress tensor within the coal pillar with dip angle 0°

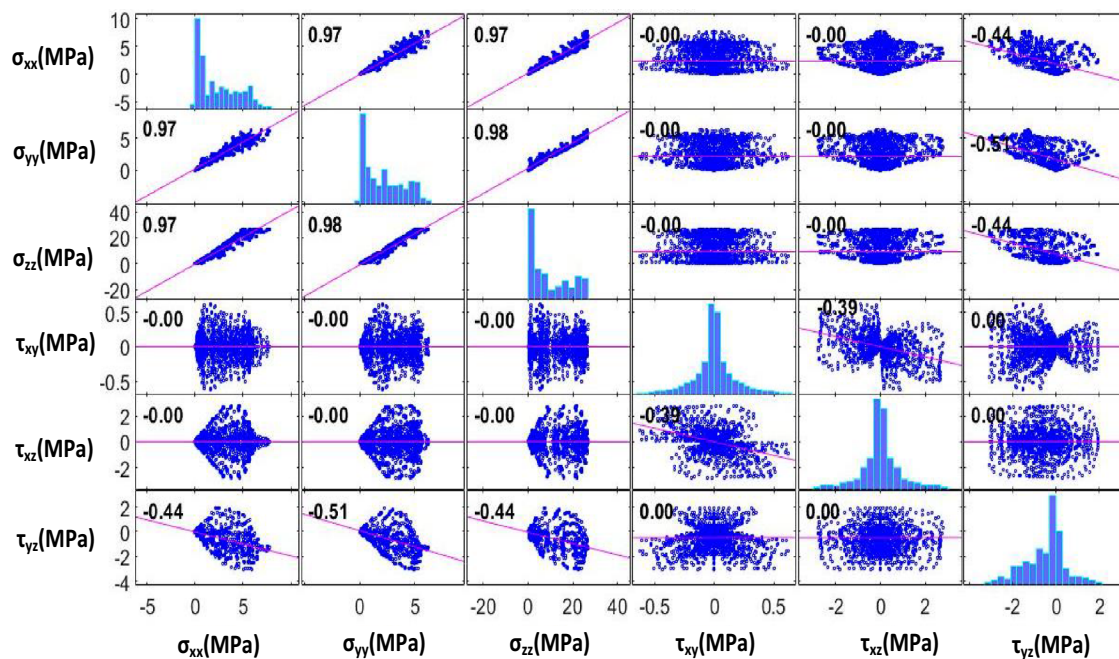


Fig. 14 Correlation matrix for the stress tensor within the coal pillar with dip angle 10°

correlation coefficients among the shear components, i.e., τ_{xy} , τ_{xz} and τ_{yz} increase with the increase of coal pillar dip angle. For example, the correlation coefficient between τ_{xy} and τ_{xz} is 0.0 and -0.89 for the coal pillar with dip angles 0° and 40° , respectively. It suggests that the shear components in the flat pillars are less compared to the inclined pillars. As the inclination of the pillars increases, the shear components

of the stress tensor become significant. This is due to the sliding tendency of the surrounding inclined rock formations along the bedding planes. As the rock easily fails in shear, the failure of the inclined pillar is governed by the induced shear stress within it.

It is found by quantifying the stress conditions with tensorial statistics that the flat pillars fail under slabbing or

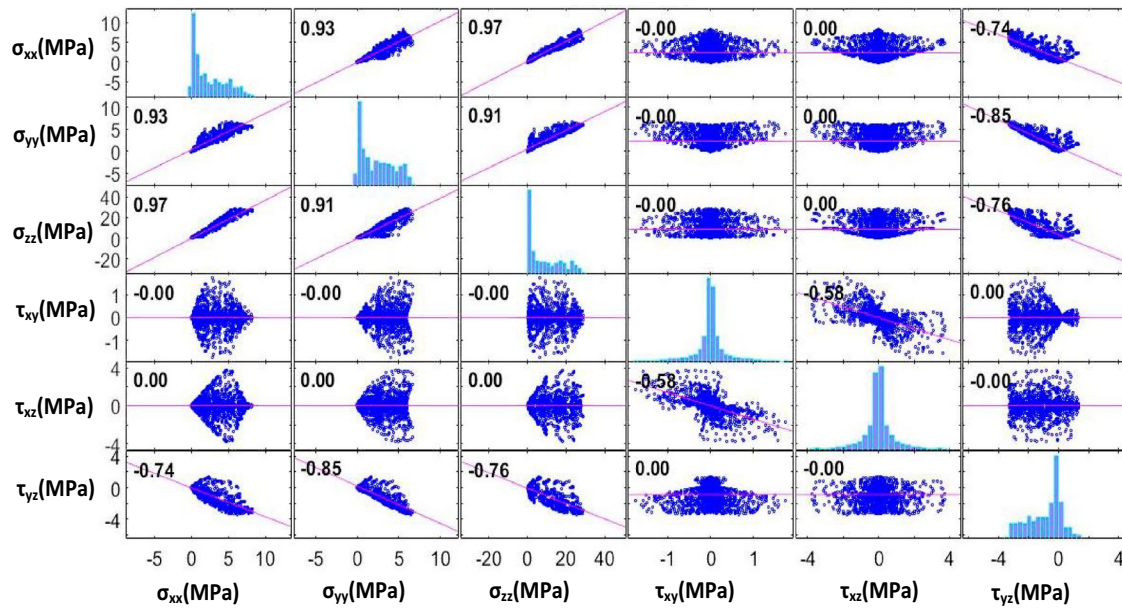


Fig. 15 Correlation matrix for the stress tensor within the coal pillar with dip angle 20°

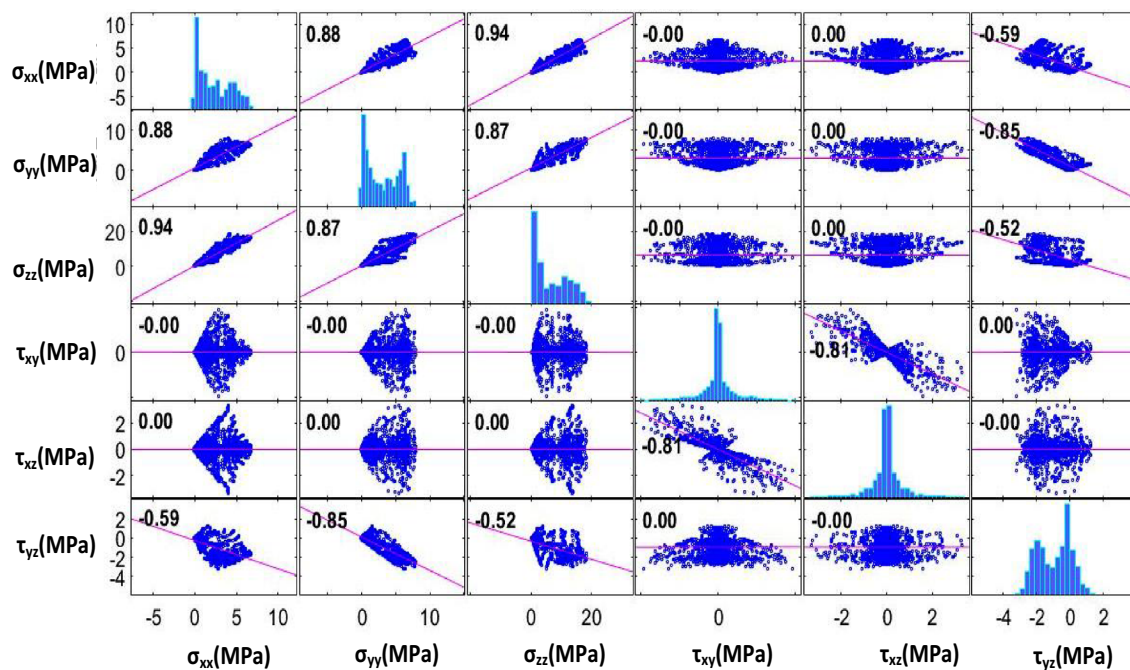


Fig. 16 Correlation matrix for the stress tensor within the coal pillar with dip angle 30°

spalling. As the correlation among the shear components of stress within the inclined coal pillars increases with the dip angle, the formation of the shear band becomes more prominent with the increase of the dip angle. The shear band propagates towards the core of the pillar with the increase

of the dip of the pillar. Thus, the inclined coal pillars fail under shear conditions. The inclined coal pillars experience high-stress conditions at the dip side which cause severe side spalling in the inclined coal pillars. Therefore, stiff supports are required to be installed at the dip side of the pillar to prevent the shearing along the bedding planes.

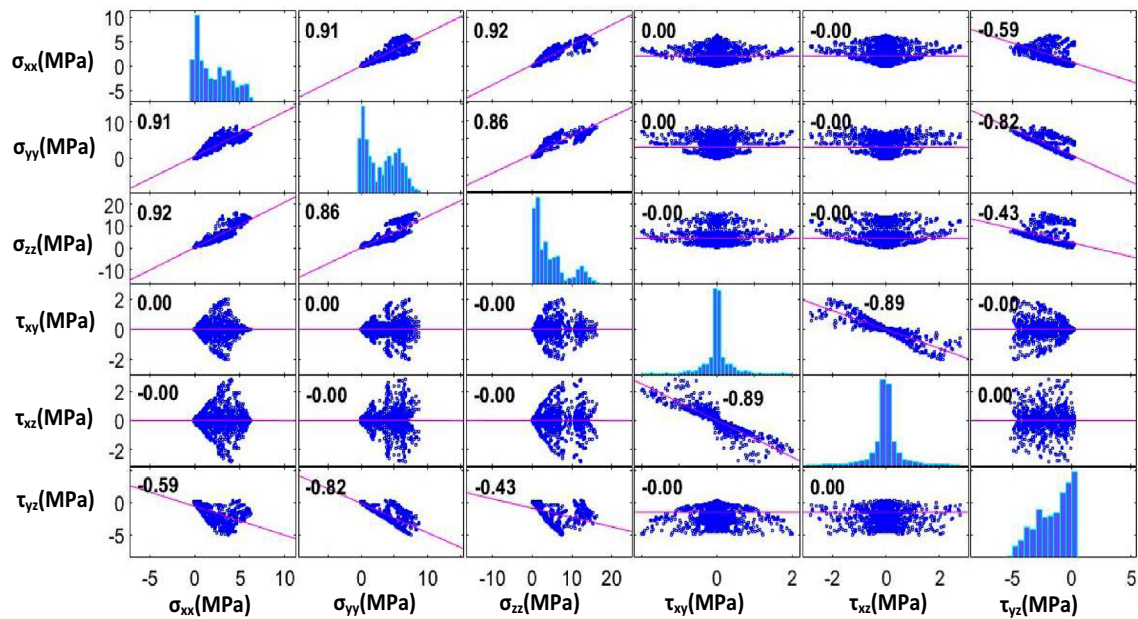


Fig. 17 Correlation matrix for the stress tensor within the coal pillar with dip angle 40°

Table 8 Orientation of the mean IPS obtained by the classical statistics and tensorial statistics for the coal pillars of different dip angles

		$\bar{\sigma}_1$		$\bar{\sigma}_2$		$\bar{\sigma}_3$	
		Azimuth (degree)	Plunge (degree)	Azimuth (degree)	Plunge (degree)	Azimuth (degree)	Plunge (degree)
Dip 0°	Classical statistics	0.37	82.85	273.92	-0.78	4.03	1.48
	Tensorial statistics	25.73	89.99	271.30	0.00	1.30	0.00
Dip 10°	Classical statistics	0.03	80.20	269.88	0.04	359.56	2.66
	Tensorial statistics	0.02	86.25	270.07	-0.00	0.07	3.74
Dip 20°	Classical statistics	0.11	74.97	269.87	1.34	359.58	0.91
	Tensorial statistics	359.95	81.99	270.28	-0.04	0.29	8.00
Dip 30°	Classical statistics	359.99	67.73	272.35	9.87	2.09	-6.61
	Tensorial statistics	359.96	75.60	270.22	0.05	359.76	14.40
Dip 40°	Classical statistics	0.01	37.79	270.62	7.25	0.894	-16.47
	Tensorial statistics	0.03	57.13	271.47	-0.93	2.08	32.85

8 Determination of the Orientation of the Mean IPS

Figures 7, 8 and 9 show the directional data, i.e. azimuth and plunge of the IPS within the coal pillars of different dip angles. The orientations of the IPS at each hexahedral zone as shown in Fig. 1 are calculated separately from the eigenvectors of the matrix T^i (Eq. 2). The orientations of the mean IPS ($\bar{\sigma}_1$, $\bar{\sigma}_2$ and $\bar{\sigma}_3$) within the inclined coal pillars are calculated by the classical statistics using Eq. (8). The tensorial statistics is also applied to obtain the orientations of the mean IPS ($\bar{\sigma}_1$, $\bar{\sigma}_2$ and $\bar{\sigma}_3$) from the eigenvectors of the matrix \bar{T} (Eq. 10). From Table 8, it is depicted that the plunge value

of the mean major IPS ($\bar{\sigma}_1$) decreases with the increase of the dip angles of the coal pillar. For example, the plunge values of the mean major IPS ($\bar{\sigma}_1$) obtained by the classical statistics are 82.85° and 37.79° whereas by the tensorial statistics are 89.99° and 57.13° for the coal pillar of dip angles 0° and 40°, respectively. Ideally, the plunge value of the mean major IPS ($\bar{\sigma}_1$) should be 90° in case of a flat coal pillar at the time of its failure. The plunge value of the mean major IPS ($\bar{\sigma}_1$) calculated by the classical statistics deviates from 90°. But, the tensorial statistical approach gives the correct result for the calculation of the orientation of the mean IPS ($\bar{\sigma}_1$, $\bar{\sigma}_2$ and $\bar{\sigma}_3$). Figure 18 shows the orientation

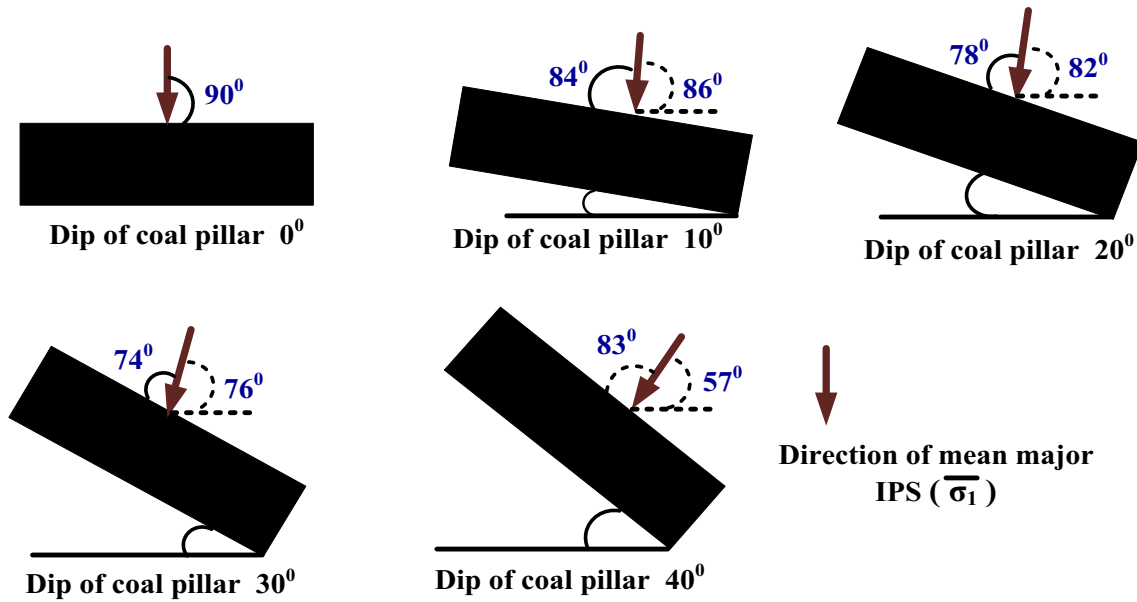


Fig. 18 Direction of the mean major IPS ($\bar{\sigma}_1$) at the time of failure of the pillar obtained by the tensorial statistics for the coal pillars of different dip angles

Table 9 Spherical variance of the orientation data of the IPS for the coal pillars of different dip angles

	σ_1	σ_2	σ_3
Dip 0°	0.03	0.44	0.45
Dip 10°	0.07	0.39	0.39
Dip 20°	0.13	0.37	0.37
Dip 30°	0.18	0.47	0.49
Dip 40°	0.43	0.42	0.42

(plunge value) of the mean major IPS ($\bar{\sigma}_1$) calculated by tensorial statistics for the coal pillars of different dip angles.

The spherical variances of the orientation data of the major IPS (σ_1) increase with the increase of coal pillar dip angle as shown in Table 9. It suggests that the orientation data of the major IPS (σ_1) within the coal pillar of dip angle 0° are more concentrated at the pole as shown in Fig. 7. The orientation data of the major IPS (σ_1) within the coal pillar of dip angle 40° are comparatively more dispersed on the surface of the unit sphere as shown in Fig. 7.

As shown in Table 8, there is a difference between the orientation data calculated by the classical statistics and by the tensorial statistics. The effectiveness of these two approaches is evaluated to identify the proper procedures of the calculation of the mean IPS ($\bar{\sigma}_1, \bar{\sigma}_2$ and $\bar{\sigma}_3$). It is a fact that the IPS i.e. σ_1, σ_2 and σ_3 are orthogonal to each other. Therefore, the orientation calculated by the classical statistics and tensorial statistics should satisfy the orthogonality of the IPS. The mean direction vector ($\tilde{\mu}$) of the IPS is expressed as follows:

$$\tilde{\mu}_i = \left[\bar{l}_i \ \bar{m}_i \ \bar{n}_i \right]^T, \tag{28}$$

where $i = 1, 2$ and 3 related to the major, intermediate and minor IPS.

To maintain the orthogonality, the dot product between the mean direction vectors of the IPS should be zero, i.e.

$$\tilde{\mu}_i \cdot \tilde{\mu}_j = 0 \ (i, j = 1, 2, 3 \text{ and } i \neq j). \tag{29}$$

It is found that the mean direction vectors obtained by the classical statistics do not satisfy Eq. (29). For example, $\tilde{\mu}_1 \cdot \tilde{\mu}_2 = 0.085, \tilde{\mu}_2 \cdot \tilde{\mu}_3 = 0.04$ and $\tilde{\mu}_3 \cdot \tilde{\mu}_1 = 0.584$ calculated by the classical statistics for the inclined coal pillar of dip angle 40°. But, the mean direction vectors calculated by the tensorial statistics satisfy Eq. (29). As the classical statistics separately evaluates the IPS, the orthogonality among them does not exist. Therefore, it can be concluded that the tensorial statistics is more accurate to calculate the mean IPS ($\bar{\sigma}_1, \bar{\sigma}_2$ and $\bar{\sigma}_3$) conditions within the coal pillars.

9 Validation by the Field Measured Data

The actual stress measurement data from various Indian underground coal mines are used to validate the failure analysis results of the inclined coal pillar obtained by numerical simulation and tensorial statistics. The stress capsules with vibrating wire sensors are installed inside the coal pillar by drilling horizontal holes. It measures the change of induced

Fig. 19 **a** Coal pillar of underground coal mines at 3 and 4 incline mine, Jhanjra, **b** installation of stress capsule in the coal pillar of 3 and 4 incline mine, Jhanjra



stress during the extraction by the caving method of mining. Figure 19 illustrates the installation of the stress capsule in the coal pillar of 3 and 4 Incline mine, Jhanjra. Field investigations (Das et al. 2019a, b; Singh et al. 2011) were carried out to collect the relevant geominig parameters and stress monitoring data from different underground coal mines, i.e. SRP-1 mine, SRP-3A mine, RK-8 mine, GDK-2 mine, GDK-5 mine of SCCL, Chirimiri Colliery, Churcha Colliery, Nowrozabad East Colliery, Rajnagar Colliery of South Eastern Coalfields Limited (SECL) and 3 and 4 Incline Jhanjra Project Colliery of Eastern Coalfields Limited (ECL). Figure 20 shows the induced stress measurement data in the coal pillars/remnants during the depillaring with the caving method. It is found that the induced stress values increase as the extraction line (goaf edge) comes closer to the pillars/remnants. The maximum stress is observed when the pillars/remnants are at the goaf. From the field investigation and the readings of the stress capsule, it is found that the stress value is maximum when the pillars/remnants are on the verge of failure. As these are the failed pillars/remnants, the safety factor of these pillars/remnants is supposed to be less than 1.0. The tensorial statistics, as well as the classical statistical approach, is applied to calculate the mean major IPS ($\bar{\sigma}_1$) at the time of failure, i.e. the strength by numerical modelling. The safety factor is calculated by dividing the mean major IPS ($\bar{\sigma}_1$) with the pillar load, which is calculated from the stress monitoring data. Table 10 shows the geominig conditions and the safety factors of the failed inclined pillars/remnants calculated by the tensorial as well as classical statistical approaches. It is found that the safety factor calculated by the classical statistical approach is more than 1.0 for three cases out of ten failed pillar cases. It suggests that the classical statistical approach does not predict the failed pillar cases correctly. But, all the failed pillar cases

are correctly predicted by the tensorial statistical approach where the safety factors of all failed cases are less than 1.0.

10 Conclusions

A comprehensive analysis is done to understand this complex failure mechanism using elasto-plastic numerical modelling as well as tensorial statistics to address the instability issues of inclined coal pillars during underground mining. The results of the study are validated with the field measurement data of failure cases of the underground coal mines in India.

It is found that the stress states of the coal pillar, at the time of its failure, are better represented by the Induced Principal Stresses (IPS). The IPS exhibit spatial variability in terms of magnitudes and directions within a coal pillar. Though the variability exists, a particular value of the IPS should be calculated to identify the failure stress state of a coal pillar. The failure stress state has been characterised by the magnitudes and the direction of the mean IPS ($\bar{\sigma}_1$, $\bar{\sigma}_2$ and $\bar{\sigma}_3$). In this study, the tensorial and classical statistics are applied to quantify the magnitudes and the direction of the mean IPS ($\bar{\sigma}_1$, $\bar{\sigma}_2$ and $\bar{\sigma}_3$) within the inclined coal pillars at the onset of failure.

It is obtained from the study that the tensorial statistics is comparatively effective to quantify the magnitudes and the direction of the mean IPS ($\bar{\sigma}_1$, $\bar{\sigma}_2$ and $\bar{\sigma}_3$). Because the mean IPS ($\bar{\sigma}_1$, $\bar{\sigma}_2$ and $\bar{\sigma}_3$) obtained by the tensorial statistics satisfy the orthogonality between each other. The magnitude of the mean major IPS ($\bar{\sigma}_1$) at the time of failure, i.e. the strength of the pillar decreases with the increase of the coal pillar dip angle. It signifies that the inclined coal pillars of the

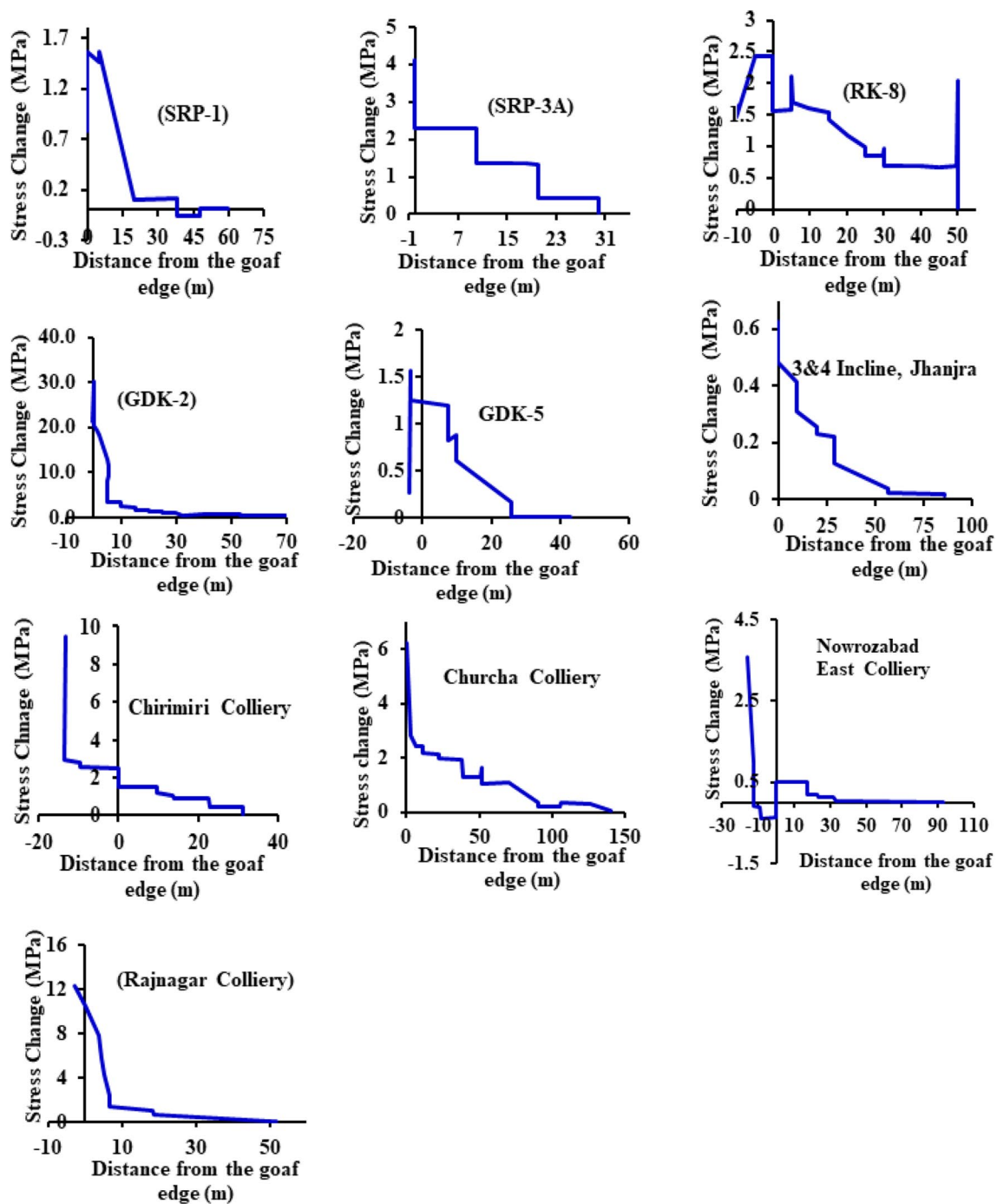


Fig. 20 Measurement of change of stress in different underground coal mines during the extraction of the pillars (Das et al. 2019a, b; Singh et al. 2011)

same dimensions as the flat coal pillars fail comparatively in less stress. The correlation coefficients among the shear components i.e., τ_{xy} , τ_{xz} and τ_{yz} increase with the increase of the dip angle of the pillar. This phenomenon shows the increase of the shear components with the dip of the coal pillar during its failure. Therefore, the inclined coal pillars

are more susceptible to shear failure. The variation of the stress tensor within the inclined coal pillars are calculated by the Euclidean dispersion (Ω_{Ed}), total variation (Ω_{total}) generalised variance (Ω_g) and effective variance (Ω_{eff}). The variance of the stress-tensor matrix of an inclined pillar is less compared to the flat pillars.

Table 10 Failed coal pillar cases

Sl. no	Mine (seam)	Depth (m)	Pillar/remnant height (m)	Pillar/remnant width (m)	Dip (degree)	In situ stress ratio (k)	Roadway width (m)	UCS of coal (MPa)	Load on the pillar/remnant (MPa)	Strength by tensorial statistics (MPa)	Safety factor by tensorial statistics	Strength by classical statistics (MPa)	Safety factor by classical statistics*
1.	SRP-1 mine (3B seam)	95	2.0	3.0×7.15	22.0	2.1	4.2	27.6	5.97	4.98	0.83	6.41	1.07
2.	SRP-3A mine (No. 1 seam)	103	1.8	2.0×7.15	18.3	1.33	4.2	8.3	8.21	1.26	0.15	2.98	0.36
3.	RK-8 mine (No. 4 seam)	65	1.8	2.0×9.2	14.0	1.9	3.6	18.3	4.85	4.25	0.88	5.92	1.22
4.	GDK-2 mine (No. 3A seam)	235	1.5	2.5×13.15	12.4	0.81	4.5	8.1	38.1	4.98	0.13	5.64	0.15
5.	GDK-5 mine (No. 4 seam)	44.3	2.4	2.5×8.0	10.3	2.57	4.2	17.4	6.42	3.86	0.6	5.71	0.89
6.	3&4 Jhanjra (RVIIA seam)	208	2.0	4.9×8.25×9.6 Triangular shaped	3.57	0.86	6.0	24.23	8.96	6.95	0.77	7.6	0.85
7.	Chirimiri Colliery (Zero seam)	91	2.5	3.0×8.75	0.0	1.45	4.5	43.4	12.96	9.5	0.73	10.24	0.79
8.	Chureha Colliery (V seam)	244	3.0	3.5×17.6	5.7	0.79	4.8	20.08	14.03	5.44	0.39	6.35	0.45
98.	Nowrozabad East Colliery (Johila Seam)	80	3.5	3.0×12.5	8.13	1.6	5.0	30.0	6.68	5.42	0.81	6.89	1.03
10.	Rajnagar Colliery (4A Seam)	172	2.5	3×15.25	4.27	0.96	4.5	41.93	18.09	9.73	0.54	11.11	0.61

*Safety factor values denoted in bold represent incorrect predictions

Table 11 Covariance (MPa^2) matrix for the stress tensor within the coal pillar with dip angle 0°

	σ_{xx} (MPa)	τ_{xy} (MPa)	τ_{xz} (MPa)	σ_{yy} (MPa)	τ_{yz} (MPa)	σ_{zz} (MPa)
σ_{xx} (MPa)	3.79	- 0.00	0.00	3.59	- 0.00	16.48
τ_{xy} (MPa)		0.02	- 0.00	- 0.00	0.00	-0.00
τ_{xz} (MPa)			0.71	0.00	0.00	0.00
σ_{yy} (MPa)				3.62	- 0.00	16.14
τ_{yz} (MPa)	Symmetry				0.69	- 0.01
σ_{zz} (MPa)						77.99

Table 12 Covariance matrix (MPa^2) for the stress tensor within the coal pillar with dip angle 10°

	σ_{xx} (MPa)	τ_{xy} (MPa)	τ_{xz} (MPa)	σ_{yy} (MPa)	τ_{yz} (MPa)	σ_{zz} (MPa)
σ_{xx} (MPa)	4.28	- 0.00	- 0.00	3.595	- 0.83	17.80
τ_{xy} (MPa)		0.03	- 0.06	- 0.00	0.00	- 0.00
τ_{xz} (MPa)			0.78	- 0.00	0.00	- 0.00
σ_{yy} (MPa)				3.23	- 0.84	15.53
τ_{yz} (MPa)	Symmetry				0.83	- 3.57
σ_{zz} (MPa)						74.73

Table 13 Covariance matrix (MPa^2) for the stress tensor within the coal pillar with dip angle 20°

	σ_{xx} (MPa)	τ_{xy} (MPa)	τ_{xz} (MPa)	σ_{yy} (MPa)	τ_{yz} (MPa)	σ_{zz} (MPa)
σ_{xx} (MPa)	4.91	- 0.00	0.00	4.03	- 1.80	18.24
τ_{xy} (MPa)		0.14	- 0.20	- 0.00	0.00	- 0.00
τ_{xz} (MPa)			0.85	0.00	- 0.00	0.00
σ_{yy} (MPa)				3.86	- 1.82	15.20
τ_{yz} (MPa)	Symmetry				1.19	- 7.00
σ_{zz} (MPa)						71.78

Table 14 Covariance matrix (MPa^2) for the stress tensor within the coal pillar with dip angle 30°

	σ_{xx} (MPa)	τ_{xy} (MPa)	τ_{xz} (MPa)	σ_{yy} (MPa)	τ_{yz} (MPa)	σ_{zz} (MPa)
σ_{xx} (MPa)	3.90	- 0.00	0.00	4.19	- 1.15	10.09
τ_{xy} (MPa)		0.18	- 0.25	- 0.00	0.00	- 0.00
τ_{xz} (MPa)			0.52	0.00	- 0.00	0.00
σ_{yy} (MPa)				5.76	- 2.00	11.33
τ_{yz} (MPa)	Symmetry				0.96	- 2.79
σ_{zz} (MPa)						29.53

Table 15 Covariance matrix (MPa^2) for the stress tensor within the coal pillar with dip angle 40°

	σ_{xx} (MPa)	τ_{xy} (MPa)	τ_{xz} (MPa)	σ_{yy} (MPa)	τ_{yz} (MPa)	σ_{zz} (MPa)
σ_{xx} (MPa)	3.37	0.00	- 0.00	4.13	- 1.51	7.02
τ_{xy} (MPa)		0.19	- 0.24	0.00	- 0.00	- 0.00
τ_{xz} (MPa)			0.38	- 0.00	0.00	- 0.00
σ_{yy} (MPa)				6.13	- 2.82	8.88
τ_{yz} (MPa)	Symmetry				1.93	- 2.49
σ_{zz} (MPa)						17.18

It is found that the directions of the IPS within the flat coal pillars are concentrated around the pole of a unit sphere. But as the dip of the coal pillars increases, the points are

more dispersed and shifted towards the equatorial plane. This phenomenon signifies that the direction of the mean major IPS ($\bar{\sigma}_1$) within the flat coal pillar is along the vertical

axis. As the dip of the coal pillars increases, the direction of the mean major IPS ($\bar{\sigma}_1$) deviates from the vertical axis and shifts towards the horizontal plane. Therefore, the shear stress components increase within the inclined pillars.

The failure mechanism results of the inclined pillars obtained by the numerical simulation and tensorial statistics approach are well validated by the stress measurement data in the underground coal mines. The comparison shows that all the failed pillar cases are correctly identified by the tensorial statistical approach, but some failed pillar cases are not predicted correctly by the classical statistical approach. It suggests that tensorial statistics is a more effective approach to analyse the stress state in an underground excavation. The procedures described in this paper can be applied to effectively quantify the magnitude and the direction of the mean IPS ($\bar{\sigma}_1$, $\bar{\sigma}_2$ and $\bar{\sigma}_3$) within the inclined pillars at the onset of failure. This study would help the researchers to characterise the behaviour of the inclined pillars during its failure, which would help to address the instability issues of the inclined coal pillars during the underground extraction of coal. The failure phenomena of the inclined coal pillar described in this paper and the quantification of the IPS would also help the researchers to determine the adequate size and the orientation of the inclined coal pillar for safe and efficient mining of the coal inclined coal seams.

Appendix

See Tables 11, 12, 13, 14 and 15.

Acknowledgements The authors are thankful to the Directors of CSIR-CIMFR, Dhanbad and IIT (ISM), Dhanbad for their support and encouragement for publication of this paper. This study is related to the ongoing PhD works of the first author. The views conveyed in this study are of the authors and not necessarily of the organisations/institutes with which they are associated.

Declarations

Conflict of interest The authors declare that they have no conflict of interest.

References

- Arthur JRF, del Rodriguez CJI, Dunstan T, Chua KS (1980) Principal stress rotation: a missing parameter. *J Geotech Eng* 106:419–433
- Bai Q, Tibbo M, Nasser MHB, Young RP (2019) True triaxial experimental investigation of rock response around the mine-by tunnel under an in situ 3D stress path. *Rock Mech Rock Eng* 52:3971–3986
- Bieniawski ZT (1976) Rock mass classifications in rock engineering. In: Bieniawski ZT (ed) *Exploration for rock engineering*. Balkema, Rotterdam, pp 97–106

- Brady BH, Brown ET (1993) *Rock mechanics for underground mining*, 2nd edn. Chapman and Hall
- Cantieni L, Anagnostou G (2009) The effect of the stress path on squeezing behavior in tunneling. *Rock Mech Rock Eng* 42:289–318
- Das AJ, Mandal PK, Bhattacharjee R, Tiwari S, Kushwaha A, Roy LB (2017) Evaluation of stability of underground workings for exploitation of an inclined coal seam by the ubiquitous joint model. *Int J Rock Mech Min Sci* 93:101–114
- Das AJ, Mandal PK, Paul PS, Sinha RK (2019a) Generalised analytical models for the strength of the inclined as well as the flat coal pillars using rock mass failure criterion. *Rock Mech Rock Eng* 52:3921–3946
- Das AJ, Mandal PK, Paul PS, Sinha RK, Tewari S (2019b) Assessment of the strength of inclined coal pillars through numerical modelling based on the ubiquitous joint model. *Rock Mech Rock Eng* 52:3691–3717
- Davis JC (1986) *Statistics and data analysis in geology*, 2nd edn. Wiley, New York
- Diederichs MS, Villeneuve M, Kaiser PK (2004) Stress rotation and tunnel performance in brittle rock. *Tunnelling Association of Canada Symposium*, Edmonton, p 8p
- Eberhardt E (2001) Numerical modelling of three-dimension stress rotation ahead of an advancing tunnel face. *Int J Rock Mech Min Sci* 38:499–518
- Feng Y, Harrison JP, Bozorgzadeh N (2019) Uncertainty in in-situ stress estimations: a statistical simulation to study the effect of numbers of stress measurements. *Rock Mech Rock Eng* 52:5071–5084
- Fisher NI, Lewis T, Embleton BJ (1993) *Statistical analysis of spherical data*. Cambridge University Press, p 329
- Foroughi MH (1996) Some aspects of coal pillar stability in inclined coal seams. PhD dissertation, University of New South Wales, p 273
- Gao K, Harrison JP (2017) Generation of random stress tensors. *Int J Rock Mech Min Sci* 94:18–26
- Gao K, Harrison JP (2018a) Scalar-valued measures of stress dispersion. *Int J Rock Mech Min Sci* 106:234–242
- Gao K, Harrison JP (2018b) Multivariate distribution model for stress variability characterisation. *Int J Rock Mech Min Sci* 102:144–154
- Gao K, Harrison JP (2019) Examination of mean stress calculation approaches in rock mechanics. *Rock Mech Rock Eng* 52:83–95
- Garza-Cruz T, Pierce M, Board M (2019) Effect of shear stresses on pillar stability: a back analysis of the troy mine experience to predict pillar performance at Montanore Mine. *Rock Mech Rock Eng* 52(12):4979–4996
- Han J, Zhang H, Liang B, Rong H, Lan T, Liu Y, Ren T (2016) Influence of large syncline on in situ stress field: a case study of the Kaiping Coalfield. *China Rock Mech Rock Eng* 49:4423–4440
- Horn RA, Johnson CR (2013) *Matrix analysis*, 2nd edn. Cambridge University Press, p 643
- Itasca Consulting Group, Inc. (2017) *FLAC3D (Fast Lagrangian Analysis of Continua in 3 dimensions)*. Version 5.0. Minneapolis, M
- Jessu KV, Spearing AJS (2019) Performance of inclined pillars with a major discontinuity. *Int J Min Sci Tech* 29(3):437–443
- Jessu KV, Spearing AJS, Sharifzadeh M (2018) Laboratory and numerical investigation on strength performance of inclined pillars. *Energies* 11(3229):1–17
- Jaiswal A, Shrivastva BK (2009) Numerical simulation of coal pillar strength. *Int J Rock Mech Min Sci* 46:779–788
- Johnson RA, Wichern DW (2002) *Applied multivariate statistical analysis* (Vol 5, No 8). Prentice Hall, Upper Saddle River
- Kaiser PK, Yazici S, Maloney S (2001) Mining-induced stress change and consequences of stress path on excavation stability—a case study. *Int J Rock Mech Min Sci* 38:167–180

- Koptev AI, Ershov AV, Malovichko EA (2013) The stress state of the Earth's lithosphere: results of statistical processing of the world stress-map data. *Moscow Univ Geol Bull* 68:17–25
- Kushwaha A, Banerjee G (2005) Exploitation of developed coal mine pillars by shortwall mining—a case example. *Int J Rock Mech Min Sci* 42:127–136
- Kushwaha A, Singh SK, Tewari S, Sinha A (2010) Empirical approach for designing of support system in mechanized coal pillar mining. *Int J Rock Mech Min Sci* 47:1063–1078
- Lei Q, Gao K (2019) A numerical study of stress variability in heterogeneous fractured rocks. *Int J Rock Mech Min Sci* 113:121–133
- Li Z, Zhou H, Jiang Y, Hu D, Zhang C (2019) Methodology for establishing comprehensive stress paths in rocks during hollow cylinder testing. *Rock Mech Rock Eng* 52:1055–1074
- Lorig LJ, Cabrera A (2013) Pillar strength estimates for foliated and inclined pillars in schistose material. In *Proceedings of the 3rd international FLAC/DEM symposium, Hangzhou, China*, pp 22–24
- Ma T, Wang L, Suorineni FT, Tang C (2016) Numerical analysis on failure modes and mechanisms of mine pillars under shear loading. *Shock Vib Article ID* 6195482:14
- Mandal PK, Singh R, Maiti J, Singh AK, Kumar R, Sinha A (2008) Underpinning-based simultaneous extraction of contiguous sections of a thick coal seam under weak and laminated parting. *Int J Rock Mech Min Sci* 45:11–28
- Maritz JA (2015) The effect of shear stresses on pillar strength. PhD dissertation, University of Pretoria, p 114
- Martin CD (1997) Seventeenth Canadian geotechnical colloquium: the effect of cohesion loss and stress path on brittle rock strength. *Can Geotech J* 34:698–725
- Martin D, Kaiser PK, Tannant D (1999) Stress path and failure around mine openings. In: *Proceedings of the 9th ISRM international congress on rock mechanics*, vol 1. Paris, France, Balkema, pp 311–315
- Mizzi L, Attard D, Gatt R, Dudek KK, Ellul B, Grima JN (2020) Implementation of periodic boundary conditions for loading of mechanical metamaterials and other complex geometric microstructures using finite element analysis. *Eng Comput*. <https://doi.org/10.1007/s00366-019-00910-1>
- Mohan GM, Sheorey PR, Kushwaha A (2001) Numerical estimation of pillar strength in coal mines. *Int J Rock Mech Min Sci* 38:1185–1192
- Mondal D, Roy PNS, Kumar M (2020) Monitoring the strata behavior in the Distressed Zone of a shallow Indian longwall panel with hard sandstone cover using Mine-Microseismicity and Borehole Televiewer data. *Eng Geol* 20:105593
- Peña D, Rodríguez J (2003) Descriptive measures of multivariate scatter and linear dependence. *J Multivar Anal* 85:361–374
- Ptáček J, Koníček P, Staš L, Waclawik P, Kukutsch R (2015) Rotation of principal axes and changes of stress due to mine-induced stresses. *Can Geotech J* 52:1440–1447
- Seber GA (2007) *A matrix handbook for statisticians*. Wiley, New York, p 559
- Seo HJ, Choi H, Lee IM (2016) Numerical and experimental investigation of pillar reinforcement with pressurized grouting and pre-stress. *Tunn Undergr Sp Tech* 54:35–144
- Shabanimashcool M, Li CC (2013) A numerical study of stress changes in barrier pillars and a border area in a longwall coal mine. *Int J Coal Geol* 106:39–47
- Shen WL, Bai JB, Li WF, Wang XY (2018) Prediction of relative displacement for entry roof with weak plane under the effect of mining abutment stress. *Tunn Undergr Sp Tech* 71:309–317
- Sheorey PR (1992) Pillar strength considering in situ stresses. In: Ian-nacchione AT, et al. editors. In: *Proceedings of the workshop on coal pillar mechanics and design*, USBM IC 9315, Santa Fe, pp 122–127
- Sheorey PR (1994) A theory for in situ stresses in isotropic and transversely isotropic rock. *Int J Rock Mech Min Sci* 31:23–34
- Sheorey PR (1997) *Empirical rock failure criteria*. Balkema, Rotterdam
- Sheorey PR, Das MN, Barat D, Parasad RK, Singh B (1987) Coal pillar strength estimation from failed and stable cases. *Int J Rock Mech Min Sci* 24:347–355
- Sheorey PR, Mohan MG, Sinha A (2001) Influence of elastic constants on the horizontal in situ stresses. *Int J Rock Mech Min Sci* 38:1211–1216
- Singh AK, Singh R, Maiti J, Kumar R, Mandal PK (2011) Assessment of mining induced stress development over coal pillars during depillaring. *Int J Rock Mech Min Sci* 48:805–818
- Siren T, Hakala M, Valli J, Kantia P, Hudson JA, Johansson E (2015) In situ strength and failure mechanisms of migmatitic gneiss and pegmatitic granite at the nuclear waste disposal site in Olkiluoto, Western Finland. *Int J Rock Mech Min Sci* 79:135–148
- Walker JR, Martin CD, Dzik EJ (1990) Confidence intervals for in situ stress measurements. *Int J Rock Mech Min Sci Geomech Abstr* 27:139–141
- Wang S, Li X, Wang S (2017) Separation and fracturing in overlying strata disturbed by longwall mining in a mineral deposit seam. *Eng Geol* 226:257–266
- Wang Y, He M, Yang J, Wang Q, Liu J, Tian X, Gao Y (2020) Case study on pressure-relief mining technology without advance tunneling and coal pillars in longwall mining. *Tunn Undergr Sp Tech* 97:103236
- Wu F, Deng Y, Wu J, Li B, Sha P, Guan S, Zhang K, He K, Liu H, Qiu S (2020) Stress–strain relationship in elastic stage of fractured rock mass. *Eng Geol* 268:105498
- Xu H, Arson C (2015) Mechanistic analysis of rock damage anisotropy and rotation around circular cavities. *Rock Mech Rock Eng* 48:2283–2299
- Yan H, Zhang J, Feng R, Wang W, Lan Y, Xu Z (2020) Surrounding rock failure analysis of retreating roadways and the control technique for extra-thick coal seams under fully-mechanized top caving and intensive mining conditions: a case study. *Tunn Undergr Sp Tech* 97:103241
- Yao Q, Tang C, Xia Z, Liu X, Zhu L, Chong Z, Hui X (2020) Mechanisms of failure in coal samples from underground water reservoir. *Eng Geol* 267:105494
- Zou D, Kaiser PK (1990) Determination of in situ stresses from excavation-induced stress changes. *Rock Mech Rock Eng* 23:167–184

Publisher's Note Springer Nature remains neutral with regard to jurisdictional claims in published maps and institutional affiliations.